POLITEHNICA University of Bucharest
Faculty of Power Engineering
Doctoral School of Power Engineering

Ph.D. THESIS SUMMARY

ENERGY EFFICIENCY OF TURBOMACHINE DESIGN AND OPERATION

Author: Eng. Oana – Maria E. **DUMITRESCU**

Ph.D. Supervisor: Prof. Emer. Dr. Eng. Dan Niculae **ROBESCU**

BUCHAREST
2022

POLITEHNICA University of Bucharest
Faculty of Power Engineering
Doctoral School of Power Engineering

CSUD UPB decision no. 130 from 17.06.2022

Ph.D. THESIS SUMMARY

ENERGY EFFICIENCY OF TURBOMACHINE DESIGN AND OPERATION

Author: Eng. Oana – Maria E. **DUMITRESCU**

Ph.D. Supervisor: Prof. Emer. Dr. Eng. Dan Niculae **ROBESCU**

Ph.D. Evaluation Board

President	Prof. Dr. Eng. Constantin BULAC	POLITEHNICA University of Bucharest
Ph.D. supervisor	Prof. Dr. Eng. Dan Niculae ROBESCU	POLITEHNICA University of Bucharest
Referent	Prof. Dr. Eng. Mihai ALBULESCU	Petroleum - Gas University of Ploiesti
Referent	CS I Dr. Eng. Valentin SILIVESTRU	NRDI COMOTI
Referent	Prof. Dr. Eng. Carmen GEORGESCU	POLITEHNICA University of Bucharest

Bucharest, 2022

TABLE OF CONTENTS

T* – thesis
S** – summary

Keywords: energy efficiency, turbomachinery, isentropic efficiency, CFD, genetic algorithms, parameter correlation

CHAPTER I

INTRODUCTION

The current trend in the energy industry is to increase and improve energy efficiency globally, by reducing as much as possible the operating and maintenance costs of power generating equipment's (turbo-blowers, air centrifugal compressors, screw compressor, expanders, etc.). Furthermore, due to the global increasing birth rate and the intensification of demands from the oil and gas industry, power generation companies are facing an alarming growth in energy consumption, and at the same time there is the need to reduce greenhouse gas emissions, especially carbon dioxide (CO_2) and nitrogen oxides (NOx), with a direct impact on climate change or global warming.

Turbomachines assure an important role in a wide range of applications, from air conditioning and ventilation, to marine and aeronautical propulsion, and this is due to their compactness and reliability. But the increasingly strict requirements of the industry, both of the customers who want the most efficient turbomachines and the strict environmental regulations lead to their change or adaptation to the new demands.

Among the most popular power generating equipment with high operating point efficiency, related to reduced emission are centrifugal blowers/compressors. Although this equipment is often overloaded (lower efficiency, maintenance, repairs, etc.), the costs of energy production exceed those related to equipment maintenance, representing an extremely profitable market for the energy field, and especially for centrifugal blower applications. Due to this market segment, centrifugal blower manufacturers continuously improve this equipment by increasing energy efficiency and reducing emissions, a process also sustained by the European Commission; which supports the development of new strategies to reduce greenhouse gas emissions by at least 55% by 2030 *(European Commission, 2020).*

Therefore, at the moment, the main priority is to found energy saving techniques to minimize the energy consumption associated with their operation, the exploitation of new designs that use innovative manufacturing and assembly technologies, but also opening the perspective of unconventional optimization, such as the robust one, which takes into account geometric and assembly variations right from the manufacturing stage.

One method to optimize the energy efficiency of turbomachinery is by using CFD analysis; a technique well developed by all industries, which focuses on studying fluid dynamics problems. These analyses can ensure technological optimizations of the equipment at the component level, being able to define their performances and, implicitly the energy efficiency. Moreover, it shortens the evaluation process of the designed components.

The thesis aims to contribute to the energy efficiency of a special category of turbomachines, namely centrifugal blowers; representing some of the most versatile and reliable air equipment, designed to perform in a variety of environments and applications. The wide applicability in various fields of interest, makes this equipment suitable for optimization, hence ensuring competitiveness on the market and compliance with environmental regulations. Therefore, the present thesis has as main objective the energy efficiency of centrifugal blowers, by increasing the performance and the operating range. To achieve this objective, the

optimization of the impeller by means of genetic algorithms was considered; process that involved maximizing the effectiveness of the objective function, minimizing the number of degrees of freedom, but also reducing the computational effort in the aerodynamic optimization process.

To accomplish this general objective, the current state of research in radial turbomachinery field was considered, based on which a design and optimization methodology of centrifugal impellers was developed, coupling with these processes the CFD numerical analysis (both inviscid model and RANS 3D viscous), linearized models obtained with neural models, CFD – experimental validation and identification of geometrical parameters with maximum impact on the objective function.

CHAPTER II

CURRENT STATUS OF RESEARCH IN RADIAL TURBOMACHINERY FIELD

In the design of a turbomachinery, it is necessary to understand the extreme phenomena that can affect its operation (surge and choke), the correlation of the design process with the manufacturing process (the equipment used) and the means to reduce manufacturing costs. The initial design always starts with customer requirements or marketing analysis requirements. As for the preliminary design stage of the components, is mostly based on standard meanline design method, that uses 1D calculation for all important thermodynamic values, combining fundamental design equations with empirical correlations.

Thus, the first part of this chapter addresses design principles, performance evaluation methods, along with factors and phenomena that limit the process; while the second part presents a bibliographic study on traditional blower design methods, as well as optimization methods, based on CFD techniques together with genetic algorithms and artificial neural networks.

CHAPTER III

GENERAL PROBLEMS OF MODELING AND FLUID FLOW SIMULATION IN TURBOMACHINES

In this chapter, the methodology required to perform a numerical simulation is briefly described. The main step of such an analysis is the definition of the mathematical model corresponding to the studied application. Depending on the complexity of the phenomena involved and the available computing resources, the chosen model corresponds to a certain level of reality approximation.

The next stage is the spatial discretization of the computational domain and the definition of the numerical scheme. Depending on the geometry complexity and the expectations from the problem studied, the grid type (structured, unstructured, hybrid) and its characteristics are

chosen. Before continuing with the calculation steps, the grid and the numerical scheme must be analyzed so that they ensure the stability and accuracy of the solution, which can be achieved by evaluating the following criteria: consistency, stability and convergence.

Another important role in the numerical simulation process is occupied by turbulence modeling, through which a correct and reliable solution can be obtained. The turbulence models used to describe this phenomenon are in turn limited by the available computing power. Currently, in engineering applications, the most used models are those with two transport equations, which allow both the calculation of turbulent kinetic energy and turbulent dissipation. A final step is given by the definition of boundary and initial conditions. The choice of these conditions depends on the known data of the problem and the operating conditions of the model.

CHAPTER IV

CONTRIBUTIONS REGARDING MESH INFLUENCE, NUMERICAL SCHEMES AND TURBULENCE MODELS ON CFD ANALYSIS

The study described in this chapter presents the influence of grid size, discretization schemes and turbulence models on obtaining a converse and qualitative solution for a radial impeller. Sensitivity validation of the parameters involved in the numerical simulation process plays an important role in establishing a level of accuracy as high as possible between CFD modeling and experimental validation. A first advantage offered by numerical modeling consists in obtaining an initial/final solution much faster than experimental methods, with lower costs and computational time.

To determine the influence of the factors mentioned above, numerical simulations were carried out for a centrifugal compressor with a pressure ratio of 14:1; compressor used for the TIDE detonation engine *(Drăgan, et al., 2018*). All numerical simulation were realized using Numeca Fine software.

The spatial discretization of the domain is based on a multi-block structured grid. To validate the grid size and to ensure minimal discretization errors and case convergence, a grid independence study was realized, using four different resolutions: 0.7 million, 1.5 million, 5 million and 9 million. An important parameter in evaluating the quality of the grid is $y+$ (dimensionless wall distance); the distribution of this parameter for the rotor hub and blades can be seen in Fig. 4.1. The maximum value is around 1 for all four grid sizes and was considered suitable for the turbulence models applied further.

The turbulence models applied were Spalart-Allmaras (*SA*), *v2f*, $k - \omega$ Shear Stress Transport (*SST*) and Explicit Algebraic Reynolds Stress Model *(EARSM)*. Another aspect analyzed is the importance of numerical discretization schemes, more precisely, second - order discretization schemes for central difference and upwind.

The operating point of the impeller, was chosen to ensure convergence for all the models analyzed; therefore, the rotational speed corresponding to the nominal point was used, namely 58000 rpm. To achieve convergence of the solution, the residuals were monitored, along with the mass flow rate between the inlet and outlet, as well as other parameters of interest.

The main boundary conditions imposed to define the domain are: *Domain Inlet* - total pressure: 101353 Pa, total temperature: 300 K; *Domain Outlet* – mass flow rate: 1.65 kg/s.

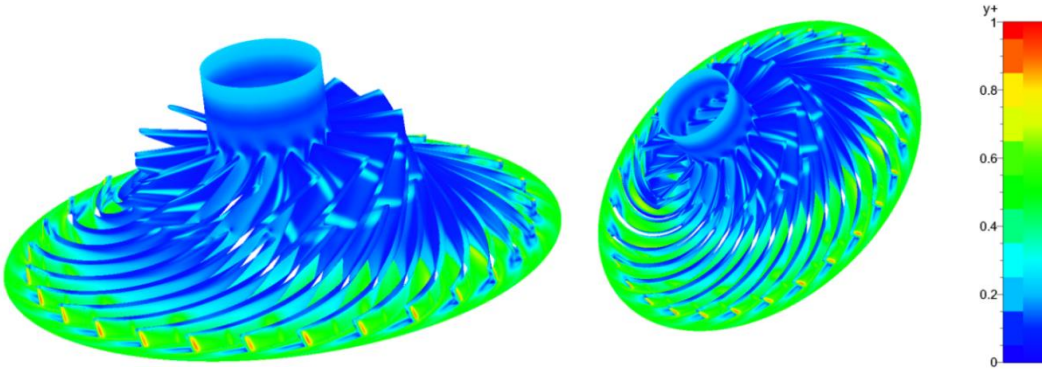

Fig. 4. 1 – *y*+ distribution on the impeller blades

Pressure ratio and isentropic efficiency were chosen as performance comparison parameters. Figure 4.2 presents the impact of the grid, discretization scheme and turbulence models on the impeller pressure ratio, highlighting the differences in stability from one grid size to another, and also between turbulence models. The *EARSM* and *v2f* models overestimate the pressure at the impeller discharge, by far compared to the rest of the models; however, as the grid size increases this numerical instability is observed for all turbulence models and numerical schemes. For the *SA* model, the most plausible results are provided by the URANS analyses corresponding to the 1.5 million grid and centered discretization scheme. The *SST* model, in turn, underestimates the pressure, especially for cases where the grid size increases above 1.5 million.

In Figure 4.3 is represented the variation of the isentropic efficiency for the turbulence models analyzed. The *EARSM* and *v2f* models overestimate the pressure ratio and implicitly the isentropic efficiency, regardless of grid resolution and numerical discretization scheme. For the two remaining models (*SA* and *SST)* and a grid size of 0.7 million, the impeller performances are higher compared to the rest of the resolutions; suggesting an overestimation of the values due to the coarse mesh. The isentropic efficiency is overestimated by up to 0.65% compared to the upwind scheme, for the *SA* turbulence model, centered scheme, with 0.7 mil elements mesh.

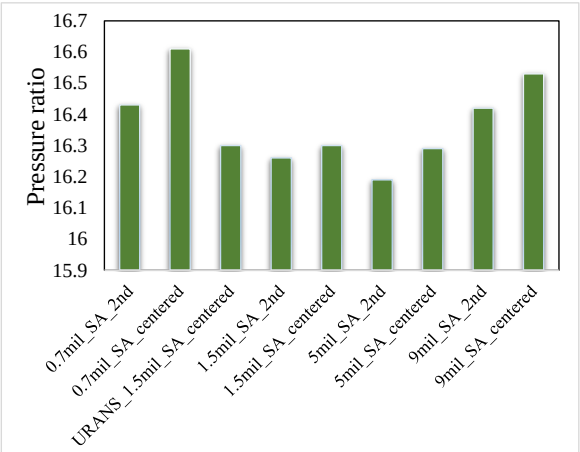

a) SA

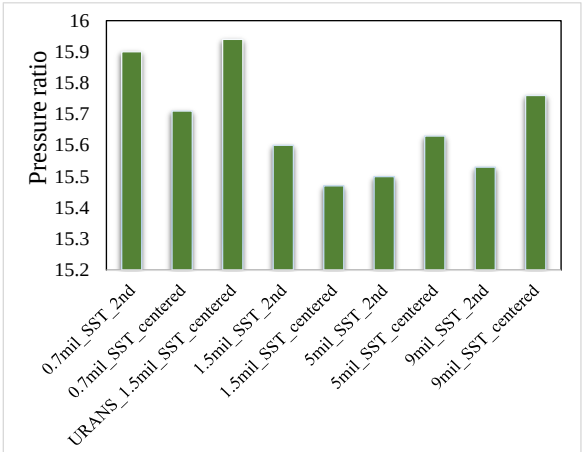

b) SST

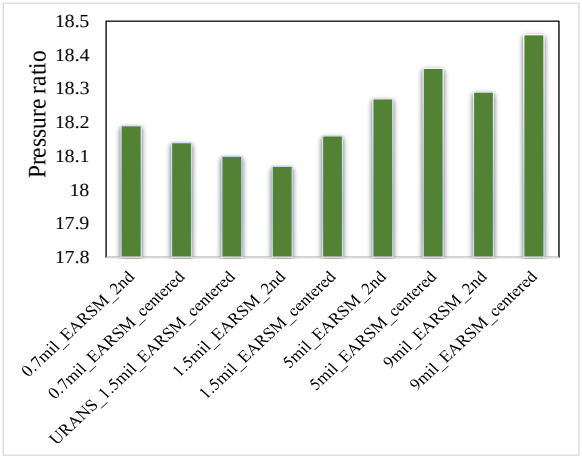

c) EARSM

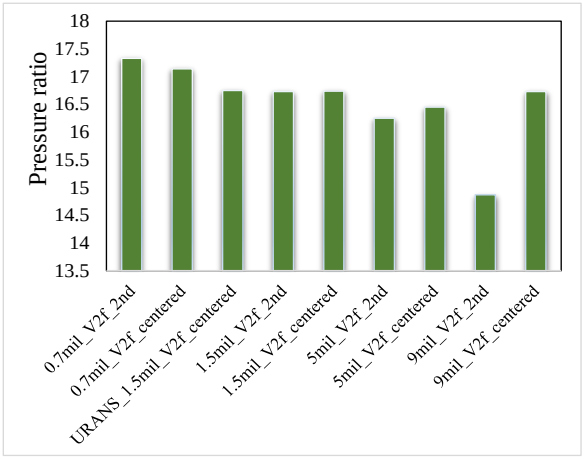

d) v2f

Fig. 4. 2 – Histograms representing the pressure ratio variation for different grid sizes, turbulence models and numerical schemes

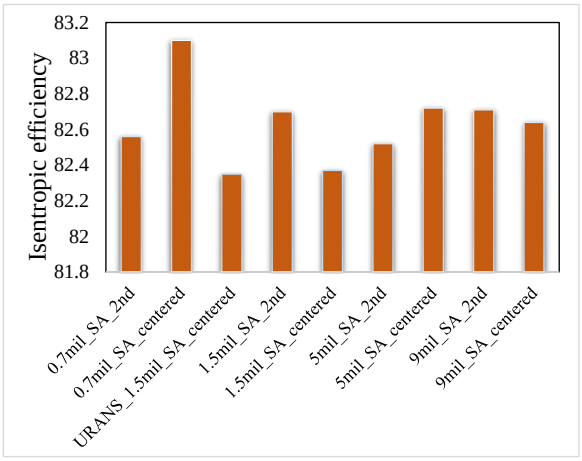

a) SA

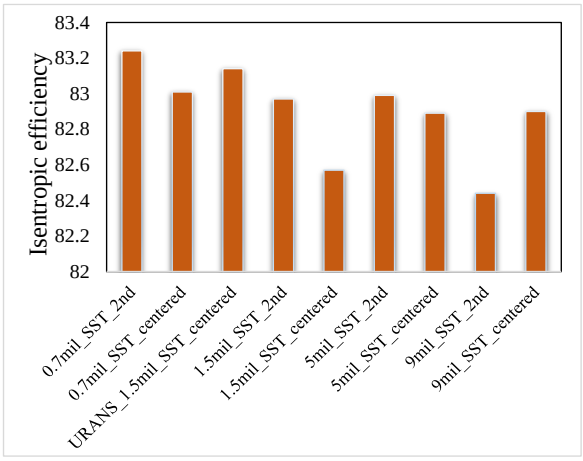

b) SST

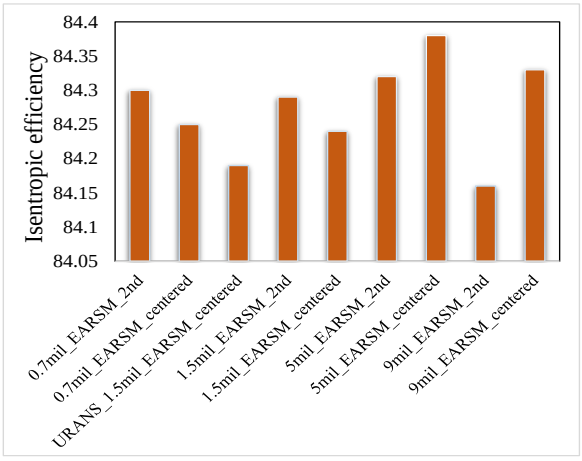

c) EARSM

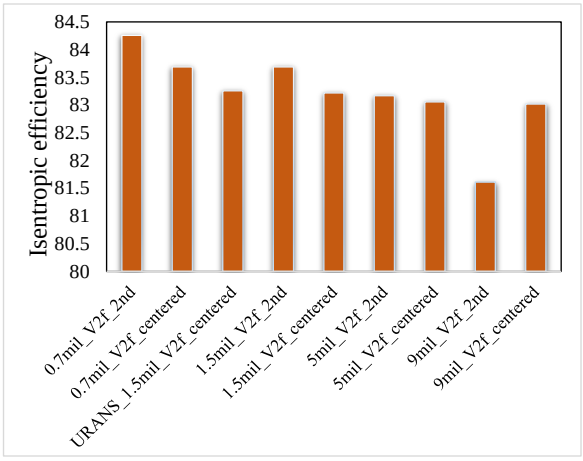

d) v2f

Fig. 4. 3 – Histograms representing the isentropic efficiency variation for different grid sizes, turbulence models and numerical schemes

According to the obtained CFD results, the excessive increase of the grid size leads to numerical instabilities of the fluid flow, therefore a grid of 1.5 million elements/channel is

considered to be sufficient to capture the phenomena that develop in the centrifugal impeller channels.

Figures 4.4 and 4.5 illustrate the variation of pressure ratio and isentropic efficiency for 1.5 million elements grid size, corresponding to the RANS analysis. The histograms compare the turbulence models and the two types of numerical discretization schemes: second - order upwind and centered differencing schemes. The *EARSM* turbulence model overestimates the rotor performance compared to the rest of the models, for both pressure ratio and efficiency. Being the only model that behaves differently for both numerical discretization schemes, it was found that for the studied case, the *EARSM* model cannot properly determine the rotor performances. Another model that leads to values of efficiency comparative to EARSM, especially for centered schemes is *v2f*. The *SA* and *SST* models offer a close estimation of efficiency, while the *SST* model underestimates the pressure ratio for both numerical schemes.

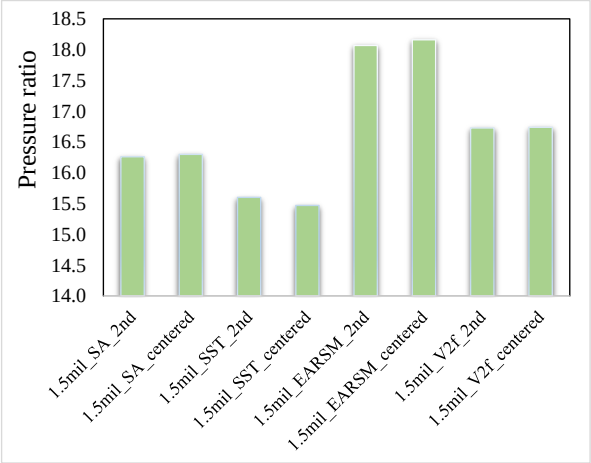

Fig. 4.4 – Impeller pressure ratio, RANS model (1.5 million grid size)

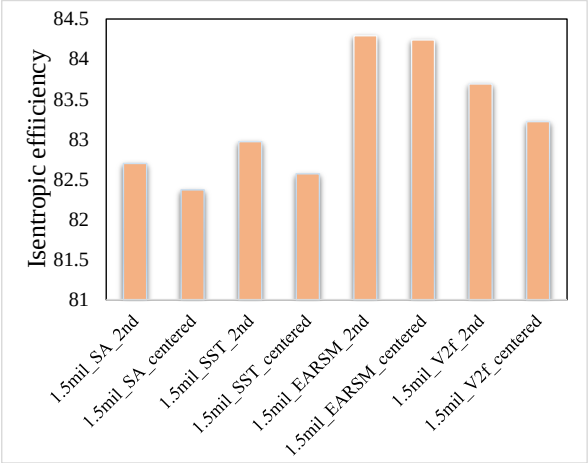

Fig. 4.5 – Impeller isentropic efficiency, RANS model (1.5 million grid size)

Another important aspect in evaluating the performance of an impeller is given by the power consumption. Following numerical simulation results, it was found that the correlation between torque, pressure ratio and efficiency depends on the turbulence model and varies with its modification, while the grid size has little impact on rotor performance, as can also be seen in Fig. 4.6 – 4.7.

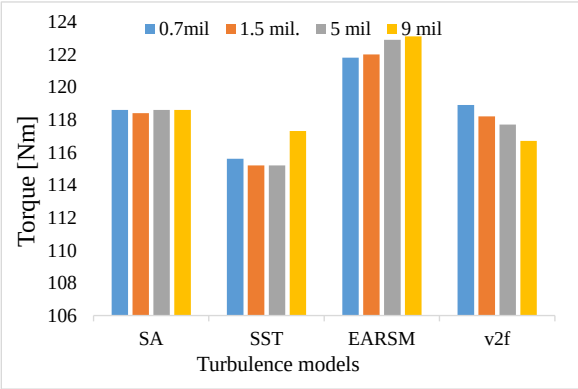

Fig. 4.6 – Impeller torque, RANS model, centered scheme

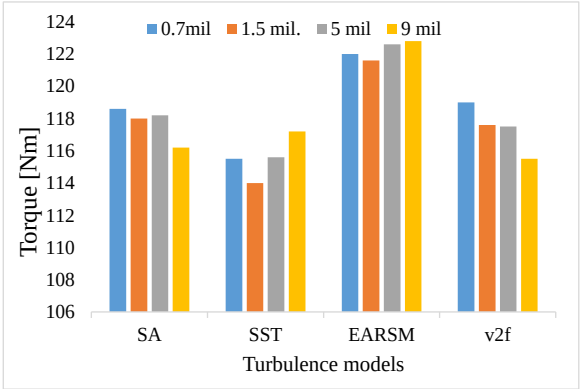

Fig. 4.7 – Impeller torque, RANS model, second-order upwind scheme

In the validation of the numerical model, the influence of second order numerical schemes (upwind and centered) was also studied. For the two numerical schemes the pressure ratio estimation is similar when the grid size is below 1.5 million; the increase of the grid resolution increases the difference between the cases. In the estimation of the isentropic efficiency, for most cases the upwind schemes overestimate its value; while for both numerical schemes the *EARSM* model leads to higher rotor performances.

A final criterion that must be mentioned is the turbulence model. Among the four models, the major differences were obtained for the *EARSM* model, overestimating both performance parameters. Due to the large differences between it and the rest of the applied models, it was considered that for such an application the model does not adequately estimate the rotor performance.

The criteria considered in this chapter represent an essential part of the method applied for the following CFD numerical analyses. Bringing these stages to a level that ensures the highest accuracy of RANS analysis is essential for the turbomachinery field, especially for cases dependent on computational effort. Thus, these analyses, in addition to establishing numerical modelling characteristics that assure accurate results, reduces the design effort through correct calculation methods that do not involve exaggerated costs, but also providing control over some detail elements that can reduce the manufacturing costs of components.

The conclusions of this chapter emphasize the importance of the numerical methods used in the simulation of the fluid flow in turbomachines, before starting the actual analysis. It is essential that, depending on the working conditions of the machine (rotational speed, pressure ratio, etc.), applicability and the computing power available, to establish what is expected from that analysis and what are the limits within which it can be achieved, so that it reflects as much as possible the actual operating conditions.

CHAPTER V

VALIDATION OF THE NUMERICAL MODEL ON CANONICAL CASES

The aim of this chapter is to validate the numerical analyzes carried out in this paper, presenting reality as accurately as possible.

In order to achieve this objective, the specialized literature was studied, selecting representative geometrical configurations of centrifugal compressors and the experimental data corresponding to it. The experimental data presented in the literature studies were compared with the results obtained from the CFD analysis, analysis carried out by the author of this thesis. If in the previous chapter the steps required to perform a numerical modelling are defined and implemented on a case study, together with the best characteristics of each step, this chapter emphasizes the method described previously and its applicability for various geometrical configurations.

In order to obtain the most accurate results, which encompass the widest range of configurations and operating range, both shrouded and unshrouded impellers have been studied; for most cases the entire compressor characteristic map was plotted.

5.1. Numerical analysis corresponding to shrouded impellers

The first two cases are focused on shrouded impellers developed and experimentally tested by Eckardt. The geometrical dimensions and experimental data can be found in *(Oh, Yoon, & Chung, 1997)*. The main differences between the cases are given by the length in the axial direction (*"O"* type: 130 mm, *"B"* type: 84.2 mm) and by the blade position at the impeller inlet. Based on this data, 3D geometries were generated and subsequently used for numerical modeling.

The input data used for the numerical simulations are: *Domain Inlet*: total pressure 101353 Pa, total temperature 288.15 K, *Domain Outlet*: mass flow rate, which varies for each working point. Also, numerical simulations were performed for different rotational speeds, namely: 10000 rpm, 12000 rpm, 14000 rpm and 16000 rpm.

5.1.1. *Impeller performance prediction* – type *"O"*

Figure 5.1 presents the impeller compression map, highlighting both the results of the numerical simulations and the experimental data corresponding to different working points. The data mentioned with *"_picCFD"* are data obtained after numerical simulation by the author, and those defined as *"_picExp"* are experimental data mentioned in paper *(Oh, Yoon, & Chung, 1997)*. For each rotational speed studied, the CFD - experimental comparison shows that: in the first part of every working line, the differences between the two analyzes are small, with values up to 4%, while in the second half the deviation increases rapidly, the error being double for some cases. The main factors driving this increase are rotational speed and flow rate. For the highest rotational speed and mass flow rate, the difference between the two evaluation methods was 8.22%.

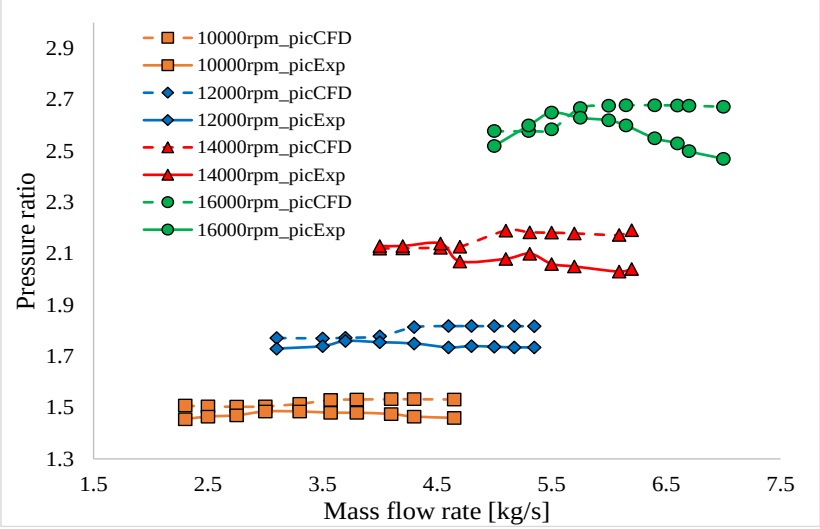

Fig. 5. 1 – Compression characteristic map of type *"O"* impeller

As for the efficiency characteristic, it is presented sequentially, separately for each rotational speed, because the differences between the values are very small, varying in the range (80 – 90 %) for efficiency and for mass flow rate between (2 – 5.5 kg/s). In this case, the major difference between the two assessment methods was obtained at the lowest rotational speed

(10000 rpm - 7.88%) and decreases with its increase (16000 rpm - 0.7%). The graphical representation of the data can be found in Fig. 5.2.

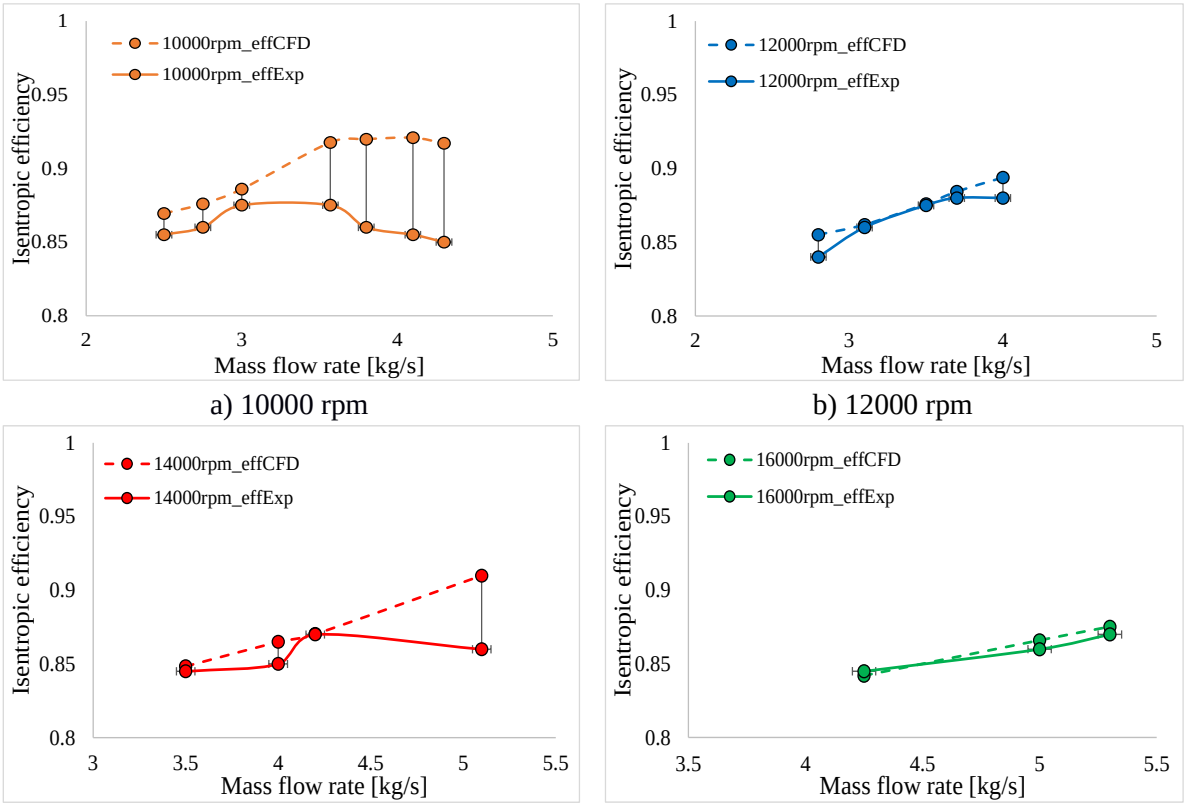

a) 10000 rpm b) 12000 rpm

c) 14000 rpm d) 16000 rpm

Fig. 5. 2 – Isentropic efficiency variation with the operating conditions

5.1.2. *Impeller performance prediction* - type *"B"*

The compression characteristic of the "B" type impeller is plotted in Fig. 5.3. If type "O" impeller in the first part of the operating range, of each rotational speed, assures small differences between the experiment and CFD data, for type "B" impeller, things are quite the opposite. For the first part of the interval, larger differences were obtained; except for the rotation speed of 10000 rpm, where the most accurate evaluation was obtained, with differences below 2.5%, for 57% of the cases. In Figure 5.3 can be observed that for the rest of the rotational speeds 12000 – 16000 rpm, the difference decrease as the flow rate increases. An aspect considered abnormal is given by the change in the slope corresponding to the CFD cases, namely, if for the first working points the CFD analysis overestimates the pressure ratio, for the last point the value is underestimated.

The numerical simulations overestimate the efficiency value, for all rotational speeds, as can be seen from Fig. 5.4. Also, the same abnormal situation of values underestimation for the maximum flow rate is maintained, and corresponds mainly to rotational speeds from 12000 rpm to 16000 rpm. Increasing the rotational speed leads to large errors; for the rotational speed of 14000 rpm was obtained the major difference, namely 8.93%. As the flow rate increases,

this value decreases to 2.83%. This is also true at 16000 rpm, where the differences between CFD and experimental decrease with increasing flow rate.

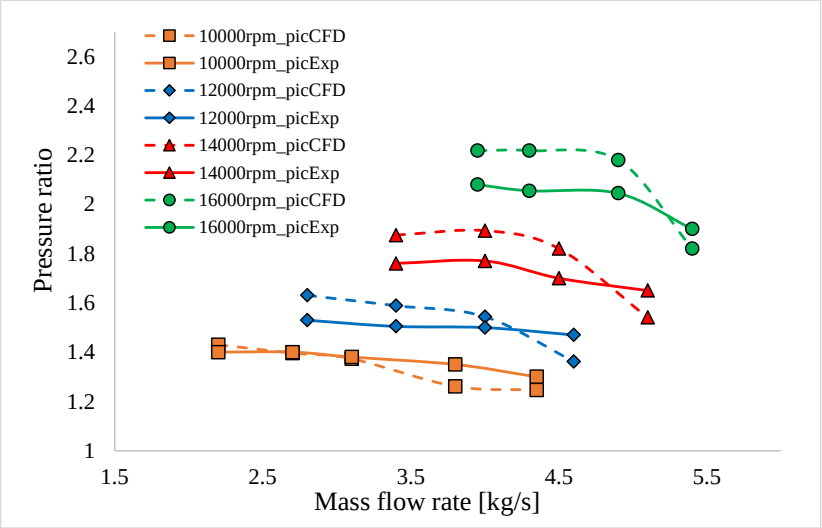

Fig. 5. 3 – Compression characteristic map of type *"B"* impeller

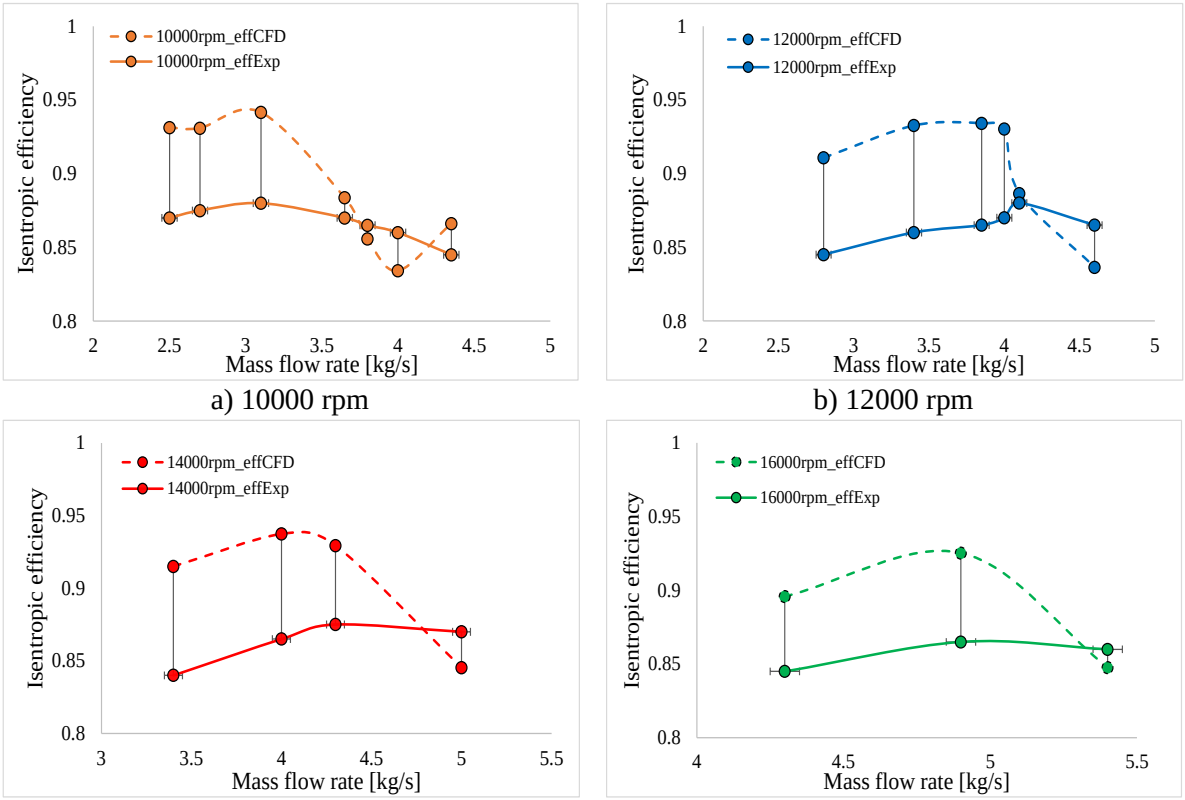

a) 10000 rpm b) 12000 rpm

c) 14000 rpm d) 16000 rpm

Fig. 5.4 – Isentropic efficiency variation with the operating conditions

For both impellers analyzed were maintained the same pre-processing conditions: same grid resolution (being generated using the same considerations: growth rate, $y+$, number of cells per height, etc.), turbulence model, numerical scheme, boundary conditions, as well as the

same way of assessing convergence. Thus, it was found that the shape of the impeller and its dimensions influence the results obtained from the CFD analysis.

For these first two impellers, it was determined that the differences between the two evaluation models are not major. If in the case of the type *"O"* impeller, the total pressure is overestimated while the efficiency is estimated accordingly, for type *"B"* rotor both parameters are overestimated. In the efficiency evaluation, for the type *"B"* impeller the higher differences are obtained for the lower values of the mass flow and are decreasing with mass flow increase. This situation is the opposite for the type *"O"* rotor; leading to a discrepancy between the two cases which can be attributed to the geometrical differences of the blade at the impeller inlet.

5.2. Numerical analysis corresponding to unshrouded impellers

5.2.1 *Performance prediction of a low-speed impeller (NASA)*

In addition of the shrouded impeller study and to extend the range of CFD – experimental data validation, the unshrouded impeller was also studied, three cases being analyzed: a low-speed rotor and a mixed compressor; the mixed compressor is modeled for two distinct values of the tip clearance (0.5 mm and 0.9 mm). The low-speed impeller was developed and tested at the NASA Lewis Research Center, and to generate the three-dimensional geometry of the rotor, the geometry data were taken from *(Hataway, 1993).*

The operating and design point of the impeller are 1862 rpm and 30 kg/s. In Fig. 5.5, the working line corresponding to this rotational speed has been defined, based on experimental data and CFD analysis results. For both parameters, pressure ratio and isentropic efficiency, the differences between the two performance evaluation methods are small, below 4%, value that reflects the impossibility of numerical simulations to exactly reproduce the conditions from the experiment. In the case of the pressure ratio, the differences between the experimental data and the CFD results are below 1%. The numerical model applied, determining with high precision the output pressure reported in the experiment.

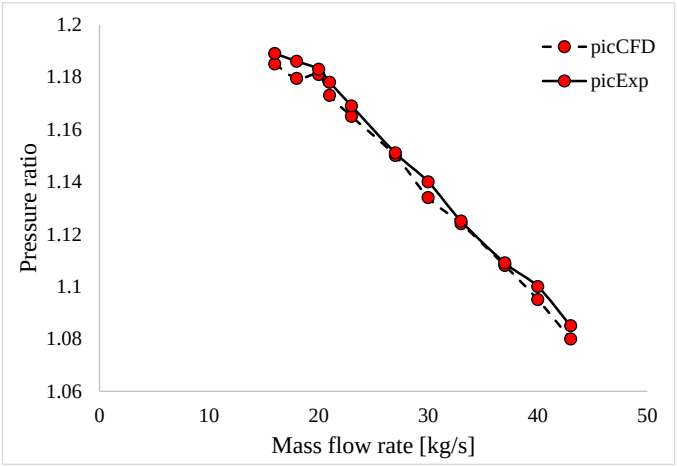

Fig. 5.5 – Impeller main working line

Regarding the efficiency evaluation, compared in Fig. 5.6, the major difference is obtained for the flow rate of 16 kg/s, namely 3.3%. Of the eleven operating points evaluated, differences below 1% are obtained for eight; and for the rest of them the maximum value is 3.31%.

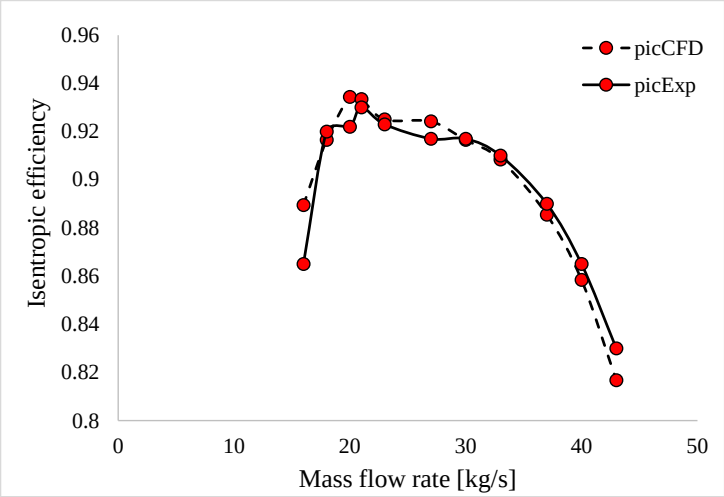

Fig. 5.6 – Isentropic efficiency variation for the main working line

The purpose of this case was to determine if for a lower speed and pressure ratio, the impeller performance was estimated closer to the experimental results, and with a higher accuracy than the previous cases. According to the results obtained (differences below 3%), we can back that up, but only for the nominal speed. Following this analysis, it can be stated that as the rotational speed and pressure ratio increase, the error also increases, and the applied turbulence model can be one of the factors that can lead to this.

5.2.2 *Performance prediction of a mixed compressor*

5.2.2.1. Tip clearance 0.5mm

A final geometry studied represents a mixed compressor stage (rotor – vaned diffuser) used for small gas turbine engines, Fig. 5.7. This compressor was designed for a rotational speed of 39836 rpm, but the experimental campaigns were carried out between 50 - 65% of the nominal speed. Also, several tip clearance values were studied to determine its influence on compressor performance and operating range. In the following, only the extreme values of the tip clearance are studied, namely (0.5 mm and 0.9 mm).

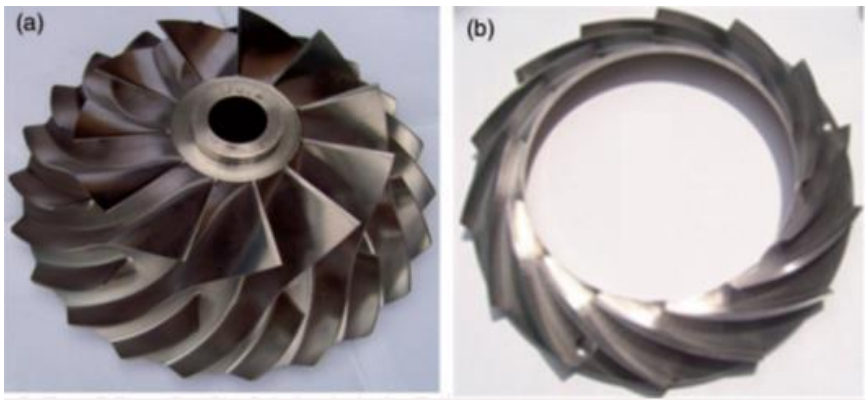

Fig. 5.7 – a) Mixed radial impeller, b) conical diffuser *(Rajakumar, Ramamurthy, & Govardhan, 2014)*

The compression characteristic is plotted in Fig. 5.8, where both the CFD cases and the experimental data, from the paper *(Rajakumar, Ramamurthy, & Govardhan, 2014)*, are presented. Overall, the differences between the cases do not exceed 6%, value that can be justified by the mathematical model applied, the differences that can appear in the generation of the CAD geometry, but also by the discrepancies obtained in the manufacturing process of the compressor components.

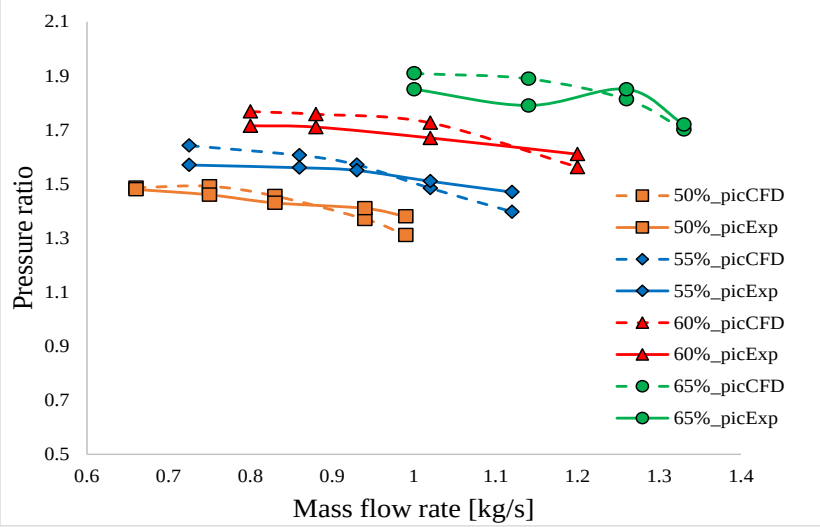

Fig. 5.8 – Compression characteristic map – tip clearance 0.5 mm

Figure 5.9 presents the values obtained for the efficiency, at 65% of the nominal speed of the compressor. In this case, the differences were below 4%; the numerical analysis providing lower efficiency values than the experimental campaign. Overall, can be determined that the numerical model applied underestimates the value of the isentropic efficiency.

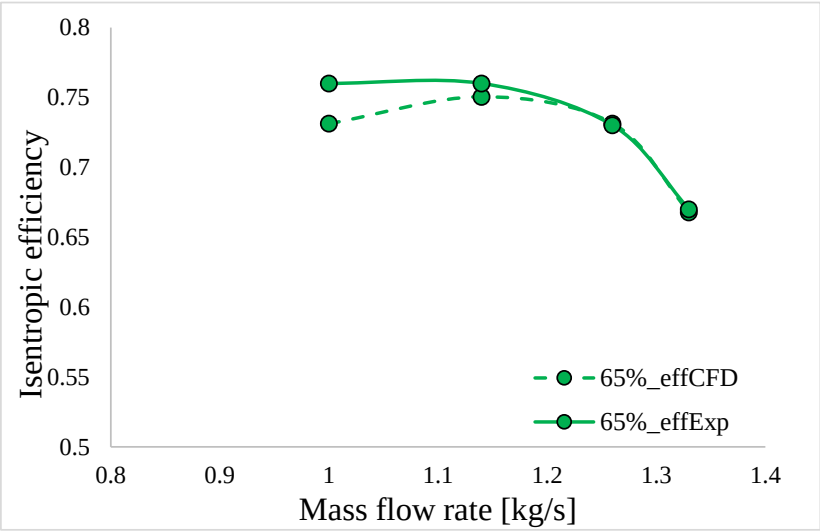

Fig. 5.9 – Isentropic efficiency variation at 65% of nominal speed

5.2.2.1. Tip clearance 0.9 mm

Increasing tip clearance by 80%, led to an increase in the differences between CFD and experimental data, by up to 1.2%. For all operating speeds and the measurement points corresponding to it, the numerical analysis overestimates the pressure ratio.

The variation of pressure ratio, defined in Fig. 5.10 shows an increase in the CFD-experimental difference as the rotational speed increases, but also a decrease as the mass flow rate increases. This decrease is best perceived at 25894 rpm (65%), with a linear variation for this operating line. For the rest of the rotational speeds, smaller differences are obtained for the points located in the middle of the working line. The extreme differences (maximum 6.72% and minimum 0.625%) being determined for the highest rotational speed values (60 – 65% of nominal speed).

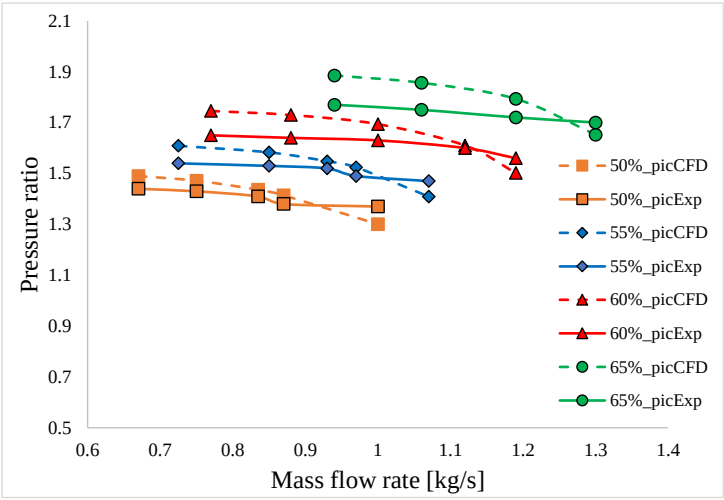

Fig. 5. 10 – Compression characteristic map – tip clearance 0.9 mm

The values obtained for the efficiency at 65% from the nominal rotational speed, are defined in Fig. 5.11. For most operating points, the numerical simulations overestimate the efficiency value. In the extreme points, were obtained discrepancies below 1%.

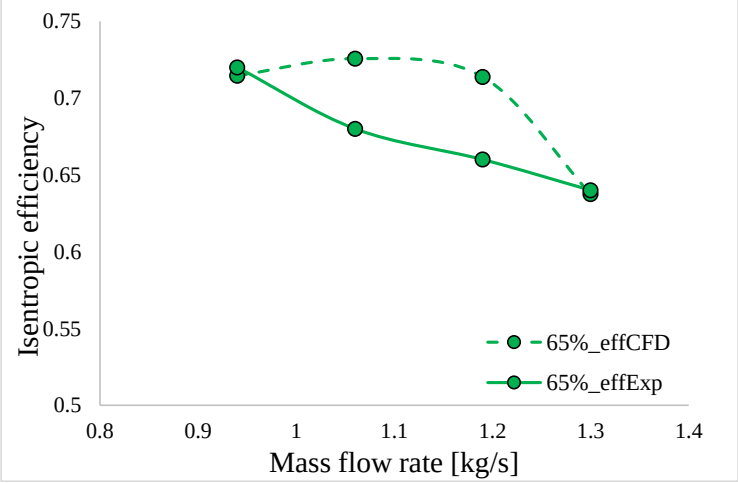

Fig. 5.11 – Isentropic efficiency variation at 65% of nominal speed

The numerical analysis of this mixed compressor shows a decrease in pressure ratio and isentropic efficiency as the tip clearance increases. This fact results from the experimental data presented by *(Rajakumar, Ramamurthy, & Govardhan, 2014)*, but also from the numerical simulations carried out. For the 0.5 mm tip clearance, increasing the rotational speed did not lead to large discrepancies between the four speeds; while, for the 0.9 mm tip clearance the differences between CFD and experimental data were increasing as rpm increased.

Comparison of CFD results with experimental data is usually used as means of validating the numerical model for the fluid velocity, pressure and temperature fields. Among the possible causes of the differences between the numerical and experimental results, we can consider both the boundary and initial conditions, but also the turbulence model used. However, the validation of the applied turbulence model is more complex. The compatibility between numerical and experimental models can be improved by using a "better" numerical model or more realistic boundary conditions.

In the cases analyzed in this chapter, the numerical model assessed the rotor performance, within a difference of less than 9%. Thus, it is considered that although changes can be made to this model, they depend on a number of factors that in turn lead to longer computing times and higher required computing power. At the same time, the results corresponding to the nominal calculation point ensure differences below 5%, which represents a realistic estimate of the performances, as far as the applicability of the RANS model is concerned.

CHAPTER VI

CONTRIBUTIONS REGARDING THE MODELING AND SIMULATION OF FLUID FLOW IN TURBOBLOWERS

The fluid flow through turbomachines represents one of the most complex processes encountered in fluid dynamics, because of the different scales at which secondary flow phenomena occur and how they interact and impact the core flow. Moreover, crossing to and from a moving frame of reference is problematic since the space in which this must occur is very tight and the flow field is heterogeneous on most of its parameters. This predisposes the case to developing numerical artifacts and so, complex interface models must be employed in the exact manner in which they were meant to be used. Since most processes involved occur at Mach numbers where compressibility effects are no longer negligible and the boundary layer is typically strained for maximum load, the turbulence model, numerical scheme, CFL number and mesh parameters are key in insuring meaningful results.

Even though computing power and more efficient solvers are becoming more available to the users, the cost of direct genetic algorithms is still prohibitive. Therefore, reduced order models are still very useful in combination with proper 3D CFD in order to maximize the performance of the designed machinery and fine tune the objective function with more subtle parameters than the classical efficiency and pressure ratio/head.

The present chapter focuses on studying the fluid flow in the impeller of a centrifugal blower, aiming at the energy efficiency of the assembly, through the geometric optimization of

the rotor, with the help of a hybrid CFD-reduced order model. The optimization process of the centrifugal blower aims at replacing the existing rotor on the blower, a shrouded-type rotor, with a new geometric configuration. The new developed geometry is obtained by studying the interaction between the defining parameters of the profile, the impeller channel and their influence on the Objective Function. The geometry defining process is followed by the modeling and simulation of the related flow, taking into account the conclusions of the study presented in Chapter IV (numerical discretization, numerical scheme, turbulence model, boundary and initial conditions, etc.).

The parameters imposed in sizing this particular centrifugal rotor are the following: total inlet pressure: 101353 Pa; total inlet temperature: 293 K; rotational speed: 25000 rpm; pressure ratio: 1.6 and mass flow rate: 3500 Nm^3/h. The rest of the parameters that are part of the design process can vary freely.

The original optimization of the rotor is made using reduced order loss models as implemented in Vista CCD, and the resulting candidates were then tested using proper RANS CFD.

Screening Optimization and MOGA (Multi-Objective Genetic Algorithm) were used as the original 1D optimization methods, and in terms of establishing the correlation between the parameters, there are two main methods that can be used: Pearson - linear correlation and Spearman - non-linear correlation.

6.1. Centrifugal blower impeller optimization

6.1.1 1D dimensioning process

Also, in order to fulfill the requirements imposed by the design settings and centrifugal blower working conditions, an objective function was imposed, defining a certain threshold that needed to be reached by every new impeller generated. The main objectives of this function were: lower aerodynamic power, pressure ratio of 1.6, the outlet Mach number less than 0.9, the absolute flow angle less than 70°.

In addition to the objective function, where selected some parameters considered representative in defining the blade geometry and their influence on the impeller performances was studied further. The parameters used in the optimization process are: P3 – number of vanes, P4 – backsweep angle, P7 – hub inlet diameter, P8 – outlet diameter, P9 – blade width, P10 – shroud inlet diameter, P12 – output Mach number, P13 – power, P14 – absolute flow angle, P15 – pressure ratio, P17 – rake angle, P19 – isentropic efficiency, P20 – meridional velocity gradient, P21 – relative velocity ratio, P22 – shroud vane normal thickness, P23 – hub blade normal thickness, P24 – tip clearance.

As a result of the 1D optimization process, for the four cases studied (100/500 samples – Screening method, 100/500 samples – MOGA method), were selected four candidates that best meet the objective imposed. Among the four candidates, based on the results, only one candidate was nominated for further 3D RANS numerical analysis.

Figure 6.1 presents the power variation for the four candidates over a 100 sample interval. As can be seen, the larger the number of samples, the wider the range of values; offering more possibilities through a more substantial discretization of the domain. The power variation for

MOGA method is closer to the minimum presenting a more complete discretization of the domain. The Screening method, in turn, although it has a wider range of variation, manages to reach local power minima close to MOGA.

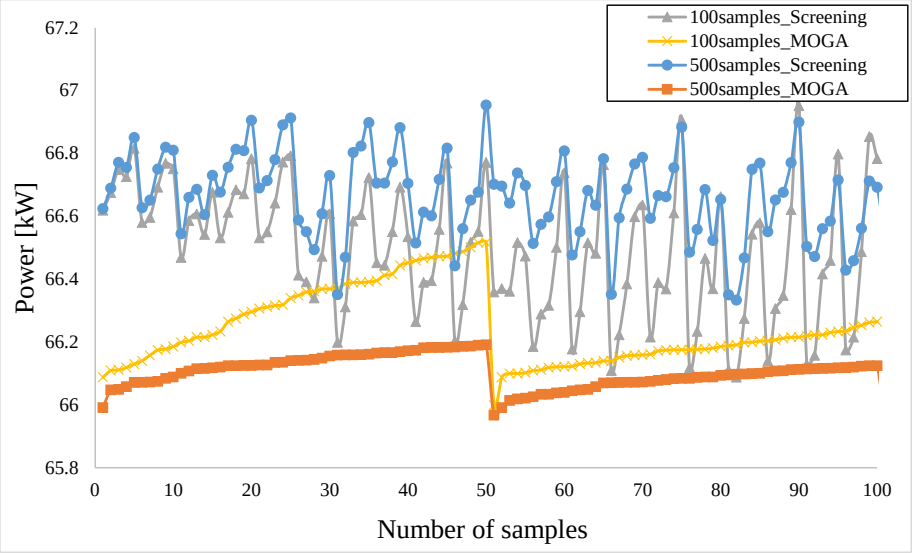

Fig. 6. 1 – Power evolution for the four cases studied

To increase the performance of the blower, an unshrouded impeller was proposed and the tip clearance was one of the parameters involved in the optimization process, Fig. 6.2. In numerical applications, its value is usually 2% of the blade height, but this value can be influenced by the loads to which the rotor is subjected; therefore, for the optimization analysis, the tip clearance varied between: 0.18 ÷ 0.22 mm. According to this graph, most of the cases generated in the optimization process consider the use of a tip clearance as small as possible, in order to obtain a high efficiency; corresponding to the range of 0.18 – 0.19 mm.

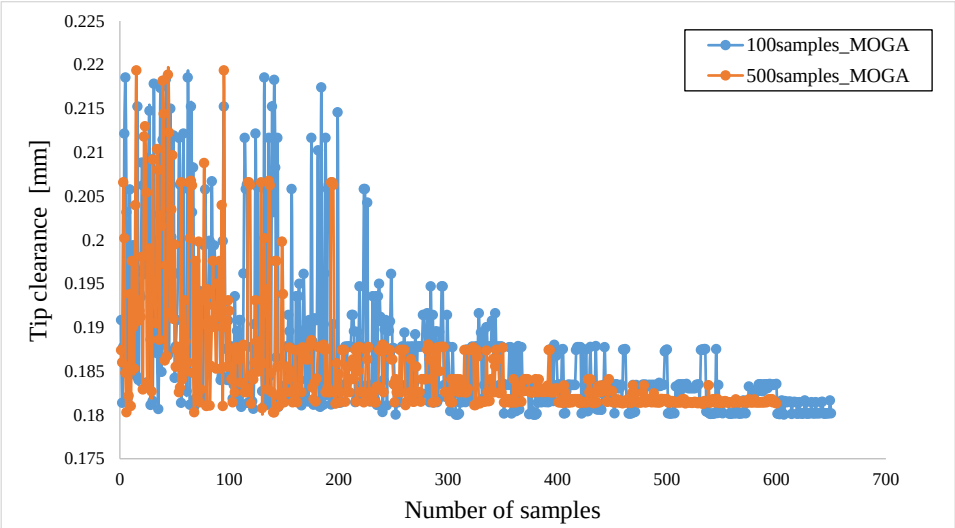

Fig. 6.2 – Tip clearance variation for the optimal candidates of the two methods

Parameters correlation

The purpose of the correlation process is to find connections between parameters considered significant in defining the rotor geometry. In this way it can be established which parameter depends on whom and how influences other quantities. The parameter correlations are only presented for the MOGA optimization procedure, as it was found that the same correlations result from both methods, only the correlation values differ very little. The purpose of the correlation process is to determine the parameters that influence each other and more precisely if similar correlations develop between both optimization methods, which have been determined.

A. *Pearson Correlation* - evaluates the linear relationship between two variables. Table 6.1 shows the Pearson correlation between the 16 parameters considered representative in the optimization process. The main diagonal has the value 1, representing the correlation of the parameter with itself; thus, the important correlations are those with values as close as possible to 1. Among the correlations close to the value 1 are (identified in the table with dark blue and shades of this color):

i. P8 – P13, P15 (outlet diameter – power, pressure ratio);
ii. P9 – P14, P19 (blade width – absolute flow angle, isentropic efficiency);
iii. P10 – P20 (shroud inlet diameter – meridional velocity gradient);
iv. P12 – P13, P15 (outlet Mach number – power, pressure ratio);
v. P14 – P19 (absolute flow angle – isentropic efficiency);
vi. P21 – P8, P12, P13, P15 (relative velocity ratio – outlet diameter, outlet Mach number, power, pressure ratio);

In addition to positively linearly correlated variables, there are also negatively linearly correlated variables (identified by the color red and its tones), such as:

i. P9 – P13, P15 (blade width – power, pressure ratio);
ii. P13 – P14 (power – absolute flow angle);
iii. P15 – P14 (pressure ratio – absolute flow angle);
iv. P19 – P8, P12 (isentropic efficiency – outlet diameter, outlet Mach number);
v. P21 – P9, P14, P19 (relative velocity ratio – blade width, absolute flow angle, isentropic efficiency) etc.

A negative correlation suggests that the two variables move in opposite directions, no link that could lead to satisfactory results can be developed between the two parameters.

B. Spearman correlation - evaluates the monotonic relationship between two variables. From Table 6.2, the following important correlations were established:

i. P9 – P13, P14, P15, P19, P21 (blade width – power, absolute flow angle, pressure ratio, isentropic efficiency, relative velocity ratio);
ii. P21 – P13, P14, P15, P19 (relative velocity ratio– power, absolute flow angle, pressure ratio, isentropic efficiency);
iii. P14 – P13, P15, P19 (absolute flow angle – power, pressure ratio, isentropic efficiency).

Table 6.1 – Linear correlation matrix, Pearson method

	P3 - NMain	P4 - BetaBlade5	P17 - RakeAngle	P20 - MerVelGrad	P21 - RelVelRatio	P22 - ThkHub	P23 - ThkShr	P24 - ClearUser	P7 - DLEhub	P8 - D5	P9 - B5	P10 - DLEshr	P12 - MachU5	P13 - Power	P14 - Alpha5rms	P15 - P05rms	P19 - EtaIsenImp
P3 - NMain	1	-0.0044	0.06144	0.00436	0.05662	-0.0387	-0.0639	-0.0432	0	-0.1006	-0.1227	0.00755	-0.1006	0.04832	-0.1461	0.04823	-0.0483
P4 - BetaBlade5	-0.0044	1	-0.0295	-0.0195	0.0068	-0.0846	-0.0358	0.0559	0	0.43943	0.23845	-0.0185	0.43943	0.00146	0.27455	0.00157	-0.0004
P17 - RakeAngle	0.06144	-0.0295	1	-0.0153	-0.0406	-0.012	0.0311	0.01104	0	-0.0438	0.06589	-0.0141	-0.0438	0.00071	0.0386	0.00085	0.0005
P20 - MerVelGrad	0.00436	-0.0195	-0.0153	1	-0.0362	0.03344	-0.0094	-0.0639	0	0.19131	-0.2287	0.99993	0.19131	0.19929	-0.226	0.19939	-0.199
P21 - RelVelRatio	0.05662	0.0068	-0.0406	-0.0362	1	-0.0214	-0.0381	0.04276	0	0.85473	-0.9289	-0.0346	0.85473	0.92961	-0.9204	0.92958	-0.9298
P22 - ThkHub	-0.0387	-0.0846	-0.012	0.03344	-0.0214	1	-0.002	0.02136	0	-0.0255	0.00429	0.03622	-0.0255	0.00342	-0.0033	0.00339	-0.0033
P23 - ThkShr	-0.0639	-0.0358	0.0311	-0.0094	-0.0381	-0.002	1	-0.0254	0	-0.0235	0.04543	-0.0101	-0.0235	-0.022	0.04378	-0.0219	0.02227
P24 - ClearUser	-0.0432	0.0559	0.01104	-0.0639	0.04276	0.02136	-0.0254	1	0	0.06783	-0.0082	-0.0652	0.06783	0.27115	-0.0015	0.27109	-0.2716
P7 - DLEhub	0	0	0	0	0	0	0	0	1	0	0	0	0	0	0	0	0
P8 - D5	-0.1006	0.43943	-0.0438	0.19131	0.85473	-0.0255	-0.0235	0.06783	0	1	-0.735	0.19249	1	0.85913	-0.7081	0.8592	-0.8587
P9 - B5	-0.1227	0.23845	0.06589	-0.2287	-0.9289	0.00429	0.04543	-0.0082	0	-0.735	1	-0.2301	-0.735	-0.9208	0.99733	-0.9207	0.92129
P10 - DLEshr	0.00755	-0.0185	-0.0141	0.99993	-0.0346	0.03622	-0.0101	-0.0652	0	0.19249	-0.2301	1	0.19249	0.20007	-0.2274	0.20017	-0.1998
P12 - MachU5	-0.1006	0.43943	-0.0438	0.19131	0.85473	-0.0255	-0.0235	0.06783	0	1	-0.735	0.19249	1	0.85913	-0.7081	0.8592	-0.8587
P13 - Power	0.04832	0.00146	0.00071	0.19929	0.92961	0.00342	-0.022	0.27115	0	0.85913	-0.9208	0.20007	0.85913	1	-0.9135	1	-1
P14 - Alpha5rms	-0.1461	0.27455	0.0386	-0.226	-0.9204	-0.0033	0.04378	-0.0015	0	-0.7081	0.99733	-0.2274	-0.7081	-0.9135	1	-0.9135	0.91398
P15 - P05rms	0.04823	0.00157	0.00085	0.19939	0.92958	0.00339	-0.0219	0.27109	0	0.8592	-0.9207	0.20017	0.8592	1	-0.9135	1	-1
P19 - EtaIsenImp	-0.0483	-0.0004	0.0005	-0.199	-0.9298	-0.0033	0.02227	-0.2716	0	-0.8587	0.92129	-0.1998	-0.8587	-1	0.91398	-1	1

Table 6.2 – Quadratic correlation matrix, Spearman method

	P3 - NMain	P4 - BetaBlade5	P17 - RakeAngle	P20 - MerVelGrad	P21 - RelVelRatio	P22 - ThkHub	P23 - ThkShr	P24 - ClearUser	P7 - DLEhub	P8 - D5	P9 - B5	P10 - DLEshr	P12 - MachU5	P13 - Power	P14 - Alpha5rms	P15 - P05rms	P19 - EtaIsenImp
P3 - NMain	1	0.03401	0.00471	0.05685	0.00967	0.00154	0.0265	0.00438	1	0.01183	0.04487	0.0582	0.01183	0.01667	0.05384	0.01662	0.01682
P4 - BetaBlade5	0.00677	1	0.00165	0.03794	0.00926	0.00717	0.04134	0.00376	1	0.20764	0.07697	0.0388	0.20764	0.02235	0.09512	0.02233	0.02243
P17 - RakeAngle	0.00452	0.00477	1	0.02496	0.0017	0.08464	0.05778	0.00084	1	0.00192	0.00718	0.02512	0.00192	0.001	0.00421	0.00099	0.00101
P20 - MerVelGrad	0.06616	0.00636	0.01025	1	0.01494	0.05891	0.00306	0.0133	1	0.04517	0.06318	1	0.04517	0.04345	0.06329	0.04347	0.04336
P21 - RelVelRatio	0.00322	0.02664	0.19974	0.00466	1	0.00179	0.01851	0.00205	1	0.73696	0.87505	0.00453	0.73696	0.86833	0.85227	0.86832	0.86851
P22 - ThkHub	0.00181	0.00723	0.01529	0.00121	0.0115	1	0.03855	0.00393	1	0.00747	0.00833	0.00142	0.00747	0.00133	0.00917	0.00134	0.00136
P23 - ThkShr	0.03542	0.01713	0.04425	0.00884	0.00843	0.00312	1	0.05084	1	0.01731	0.01037	0.00934	0.01731	0.03338	0.00945	0.03339	0.03322
P24 - ClearUser	0.00231	0.03	0.0004	0.02707	0.07051	0.00405	0.00843	1	1	0.0506	0.09144	0.02701	0.0506	0.16094	0.0973	0.16086	0.16117
P7 - DLEhub	0	0	0	0	0	0	0	0	0	0	0	0	0	0	0	0	0
P8 - D5	0.01278	0.20541	0.0884	0.0388	0.74492	0.00426	0.02174	0.01923	1	1	0.57523	0.03945	1	0.73997	0.53065	0.74009	0.7391
P9 - B5	0.04889	0.05742	0.2048	0.05358	0.86739	0.0104	0.00371	0.0023	1	0.54123	1	0.05412	0.54123	0.863	0.99837	0.86296	0.86354
P10 - DLEshr	0.06612	0.00671	0.01117	1	0.01529	0.05556	0.00348	0.01467	1	0.04548	0.06346	1	0.04548	0.04335	0.06357	0.04337	0.04326
P12 - MachU5	0.01278	0.20541	0.0884	0.0388	0.74492	0.00426	0.02174	0.01923	1	1	0.57523	0.03945	1	0.73997	0.53065	0.74009	0.7391
P13 - Power	0.00254	0.14351	0.18283	0.04718	0.87094	0.00071	0.0127	0.09537	1	0.75904	0.88426	0.04744	0.75904	1	0.86249	1	1
P14 - Alpha5rms	0.06425	0.0765	0.18814	0.05164	0.84711	0.01047	0.00314	7.23E-05	1	0.50321	0.9986	0.05223	0.50321	0.83607	1	0.83601	0.83678
P15 - P05rms	0.00253	0.1435	0.18275	0.04723	0.87094	0.00075	0.01267	0.09538	1	0.7591	0.88427	0.04749	0.7591	1	0.8625	1	1
P19 - EtaIsenImp	0.00257	0.14297	0.18384	0.0469	0.87084	0.00069	0.01283	0.09532	1	0.75892	0.88417	0.04716	0.75892	1	0.86234	1	1

Following the results of the correlations, it was found that in defining the impeller geometry, an important role is played by the connection between parameters such as:

a) Relative velocity ratio – outlet Mach number, power, pressure ratio;

b) Meridional velocity gradient – hub inlet diameter;

c) Blade width – absolute flow angle, isentropic efficiency.

In Table 6.3, only the candidates considered optimal for the four analyzed cases are defined. The difference between the candidates varies between 0.08 – 48.5%; with major values recorded for the input parameters, such as: backsweep angle (12.55%), rake angle (33.4%), hub vane normal thickness (48.55%), shroud vane normal thickness (45.2%) and blade width (16.49%). Between the output parameters of the impeller, the differences are much smaller, having a maximum of 5.93% for the absolute flow angle, followed by outlet Mach number (1.2%), then power (0.244 %) and isentropic efficiency (0.226%). In order to determine which of the cases will be subjected to numerical CFD modeling, the requirements of the objective function were analyzed, and based on them, the candidate *500_C2_MOGA* was selected. This choice is centered on the power value, which is minim for this candidate.

Table 6.3 – Performance validation for candidates considered optimal

	P3 - NMain	P12 - MachU5	P13 - Power (kW)	P14 - Alpha5rms (degree)	P15 - P05rms (kPa)	P19 - EtaIsenImp
max	15	0.903	67.034	65.337	168.33	0.90425
100_C1_Screening	9	0.85070	66.08805	63.55748	168.24355	0.90222
100_C2_MOGA	9	0.84577	65.92820	67.29040	168.22869	0.90424
500_C1_Screening	9	0.84046	65.99145	65.37612	168.23458	0.90344
500_C2_MOGA	9	0.84666	65.92629	67.56232	168.22848	0.90426
min	9	0.765	66	49.285	168.23	0.89

[.....]

6.1.2 2D dimensioning process

The first step of the 2D process is the generation of an initial geometry by combining basic theoretical relations with empirical correlations. The 1D geometry (blade channel, blade position, diameters, etc.) is then modified using the Ansys BladeGen program, where further changes can be made to blade angles, trailing edge and leading edge shape, blade thickness, etc. At the same time, this interface provides a first three-dimensional illustration of the impeller. The next stage is the geometry parametrization, taking into account the parametric curves from the hub and shroud coupled with the distribution of the angles β and θ. The resulting geometry is initially analyzed using the Euler model (inviscid analysis), and the output parameters, considered of interest, are introduced into the penalty function, following that the MOGA or Screening optimization methods lead to optimal candidates.

Through inviscid calculations, the domain between preliminary design solutions and full 3D CFD analyses is provided. It also allows solving the circumferentially averaged inviscid Navier–Stokes equations, supplemented with established empirical models for losses and deviations. With minimal computational effort, the inviscid solutions capture features of a full 3D flow simulation, thus facilitating vane geometry optimization. This model emphasizes the region away from the wall, where the flow is fully developed, also, for the wall region it uses loss approximations based on experimental models.

The main performance parameter of the designed rotor is the isentropic efficiency, and its variation for the two cases (100 and 500 samples) and methods (Screening and MOGA) is represented in Fig. 6.3. To assess the differences, Fig. 6.3 presents only the common range of the first 100 iterations of the four cases. In the case of the MOGA method, the difference between the local maximum and minimum is small; varying between 0.86 and 0.89; while for Screening a minimum of 0.8 is reached. This value suggests that by means of the Screening method, certain weaker connections between the parameters are also determined; while the MOGA method tries to find solutions as close as possible to the objective of the imposed function.

Parameters correlation

The correlations between the parameters that define the blade shape, represent one of the main objectives of this study; and by means of the two correlations methods Pearson and

Spearman, it is possible to determine the parameters, but also their position on the blade (from the leading edge of the trailing edge).

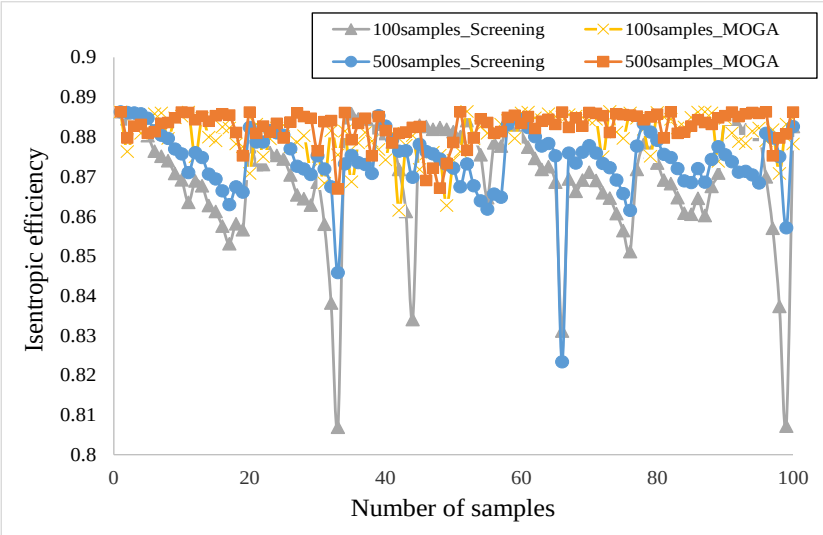

Fig. 6.3 – Isentropic efficiency variation for the cases studied

A. *Pearson correlation* - The linear parameter correlation matrix in Table 6.4 is based on the Pearson correlation, and the main positive correlations are obtained between the rotor performance parameters: P18 – P20 (isentropic efficiency – pressure ratio), P19 – P20 (power – pressure ratio) and P18 – P19 (isentropic efficiency – power). In addition to these three important connections, there are others, but they are much weaker in terms of the link between the parameters.

Also, some more pronounced negative correlations can be observed, which influence the performance parameters of the rotor in an unfavorable way (representation by a red dial). The position of these parameters is towards the trailing edge of the vane.

Table 6.4 – Linear correlation matrix, Pearson method

	P37 - Blade2.FD1016	P38 - Blade2.FD1017	P39 - Blade2.FD1018	P40 - Blade2.FD1019	P41 - Blade2.FD1020	P42 - Blade2.FD1021	P43 - Blade2.FD1022	P44 - Blade2.FD1024	P45 - Blade2.FD1026	P46 - Blade2.FD1027	P47 - Blade2.FD1028	P48 - Blade2.FD1029	P49 - Blade2.FD1030	P50 - Blade2.FD1031	P51 - Blade2.FD1032	P52 - Blade2.FD1034	P53 - NumberOfBlades.FD1	P18 - VTF etas tt	P19 - VTF power	P20 - VTF pr tt
P37 - Blade2.FD1016	1.00000	-0.03918	-0.01365	0.00920	0.00912	-0.05195	-0.00526	0.01099	-0.00494	-0.03391	0.00353	0.02343	-0.03376	0.01955	-0.01790	0.02803	-0.03261	0.03778	0.01942	0.02112
P38 - Blade2.FD1017	-0.03918	1.00000	-0.02072	0.00457	0.00356	0.02274	0.01114	-0.01279	0.00830	0.00320	-0.00274	0.00022	-0.00768	-0.00570	-0.00207	0.02492	-0.02281	0.00435	-0.01083	-0.00957
P39 - Blade2.FD1018	-0.01365	-0.02072	1.00000	0.01696	-0.00067	0.02170	0.00659	0.01446	-0.01177	-0.00435	0.01648	-0.02335	-0.01894	-0.02295	0.00664	-0.00139	0.02683	-0.10326	-0.03090	-0.03489
P40 - Blade2.FD1019	0.00920	0.00457	0.01696	1.00000	-0.00177	-0.01545	0.00724	0.00629	-0.01822	0.00534	0.01758	-0.00619	-0.02477	-0.00249	-0.05036	-0.05826	-0.05438	0.07712	0.03599	0.03229
P41 - Blade2.FD1020	0.00912	0.00356	-0.00067	-0.00177	1.00000	0.01899	-0.01442	0.00169	-0.01395	0.01316	-0.01509	0.00377	0.01599	0.00525	-0.03100	0.00433	-0.00683	-0.06532	-0.06509	-0.06699
P42 - Blade2.FD1021	-0.05195	0.02274	0.02170	-0.01545	0.01899	1.00000	0.01219	-0.00571	0.00822	0.02400	0.01724	-0.02671	-0.00669	0.00867	0.02031	-0.01274	-0.00309	-0.38903	-0.74090	-0.74204
P43 - Blade2.FD1022	-0.00526	0.01114	0.00659	0.00724	-0.01442	0.01219	1.00000	-0.00186	-0.00147	-0.02765	0.01118	0.00733	-0.02613	-0.01465	0.03615	0.01996	-0.00709	0.11560	0.22438	0.22178
P44 - Blade2.FD1024	0.01099	-0.01279	0.01446	0.00629	0.00169	-0.00571	-0.00186	1.00000	0.00949	0.02316	0.01068	-0.00805	0.00450	0.03274	0.00134	-0.00894	-0.01812	-0.30266	-0.57164	-0.57713
P45 - Blade2.FD1026	-0.00494	0.00830	-0.01177	-0.01822	-0.01395	0.00822	-0.00147	0.00949	1.00000	0.00814	0.01542	0.00342	0.01583	-0.04592	-0.00239	-0.01178	-0.00973	-0.63744	0.05956	-0.00748
P46 - Blade2.FD1027	-0.03391	0.00320	-0.00435	0.00534	0.01316	0.02400	-0.02765	0.02316	0.00814	1.00000	-0.00194	-0.02047	-0.02828	0.01605	0.01099	-0.00046	-0.00914	-0.02157	-0.02683	-0.01478
P47 - Blade2.FD1028	0.00353	-0.00274	0.01648	0.01758	-0.01509	0.01724	0.01118	0.01068	0.01542	-0.00194	1.00000	0.00055	-0.02511	-0.02514	0.02457	-0.00698	-0.02113	-0.31289	0.03460	0.00344
P48 - Blade2.FD1029	0.02343	0.00022	-0.02335	-0.00619	0.00377	-0.02671	0.00733	-0.00805	0.00342	-0.02047	0.00055	1.00000	0.00339	-0.01517	0.02082	0.01306	0.00753	0.03819	0.05265	0.05208
P49 - Blade2.FD1030	-0.03376	-0.00768	-0.01894	-0.02477	0.01599	-0.00669	-0.02613	0.00450	0.01583	-0.02828	-0.02511	0.00339	1.00000	-0.00456	0.00454	0.00101	-0.02086	0.09678	0.01780	0.01825
P50 - Blade2.FD1031	0.01955	-0.00570	-0.02295	-0.00249	0.00525	0.00867	-0.01465	0.03274	-0.04592	0.01605	-0.02514	-0.01517	-0.00456	1.00000	0.01502	0.03587	-0.01867	0.09206	0.02292	0.02612
P51 - Blade2.FD1032	-0.01790	-0.00207	0.00664	-0.05036	-0.03100	0.02031	0.03615	0.00134	-0.00239	0.01099	0.02457	0.02082	0.00454	0.01502	1.00000	0.01201	-0.01508	0.04085	0.01786	0.01804
P52 - Blade2.FD1034	0.02803	0.02492	-0.00139	-0.05826	0.00433	-0.01274	-0.01896	-0.00894	-0.01178	0.00046	-0.00698	0.01306	0.00101	0.03587	0.01201	1.00000	-0.00637	-0.03995	-0.06014	-0.06499
P53 - ExportPoints1.FD1	-0.03261	-0.02281	0.02683	-0.05438	-0.00691	-0.00309	-0.00700	-0.01802	-0.00976	-0.00979	-0.02113	0.00753	-0.02086	-0.01867	-0.01508	-0.00637	1.00000	-0.06287	-0.02439	-0.02412
P18 - VTF etas tt	0.03778	0.00435	-0.10326	0.07712	-0.06532	-0.38903	0.11560	-0.30266	-0.63744	-0.05167	-0.31289	0.03819	0.09678	0.09206	0.04085	-0.03995	-0.06287	1.00000	0.52180	0.57978
P19 - VTF power	0.01942	-0.01083	-0.03090	0.02599	-0.06509	-0.74090	0.22438	-0.57164	0.05956	0.02682	0.03460	0.05265	0.01780	0.02292	0.01786	-0.06014	-0.02439	0.52180	1.00000	0.99707
P20 - VTF pr tt	0.02112	-0.00957	-0.03489	0.03228	-0.06699	-0.74204	0.22178	-0.57713	-0.00748	0.01475	0.00344	0.05208	0.01825	0.02612	0.01804	-0.06499	-0.02412	0.57978	0.99707	1.00000

B. Spearman correlation - In addition to relationships determined by means of linear correlation, the quadratic matrix (Table 5.5) also highlights other connections between

parameters, such as: P42 – P19 and P42 – P20, where P42 represents point 4 on the X axis, used for parameterization of the model, by defining the rake angle of the blade.

Table 6.5 – Quadratic correlation matrix, Spearman method

	P37 - Blade2.FD1016	P38 - Blade2.FD1017	P39 - Blade2.FD1018	P40 - Blade2.FD1019	P41 - Blade2.FD1020	P42 - Blade2.FD1021	P43 - Blade2.FD1022	P44 - Blade2.FD1024	P45 - Blade2.FD1026	P46 - Blade2.FD1027	P47 - Blade2.FD1028	P48 - Blade2.FD1029	P49 - Blade2.FD1030	P50 - Blade2.FD1031	P51 - Blade2.FD1032	P52 - Blade2.FD1034	P53 - NumberOfBlades.FD1	P18 - VTF etas tt	P19 - VTF power	P20 - VTF pr tt
P37 - Blade2.FD1016	1.00000	0.00657	0.00034	0.00022	0.00739	0.00539	0.00060	0.00277	0.00832	0.00352	0.00001	0.00056	0.01913	0.00449	0.01096	0.03013	0.01099	0.02110	0.00060	0.00091
P38 - Blade2.FD1017	0.00237	1.00000	0.03095	0.01988	0.00140	0.00122	0.00721	0.00022	0.06017	0.00017	0.02086	0.00715	0.00534	0.00026	0.02070	0.00937	0.00456	0.00940	0.00423	0.00221
P39 - Blade2.FD1018	0.00649	0.00468	1.00000	0.01878	0.00771	0.00947	0.00281	0.00082	0.04613	0.00104	0.00492	0.02126	0.00670	0.02029	0.04295	0.01202	0.02632	0.06783	0.00607	0.00872
P40 - Blade2.FD1019	0.00009	0.00184	0.00084	1.00000	0.02519	0.00734	0.01226	0.00126	0.01746	0.00015	0.00357	0.01869	0.00772	0.08611	0.00438	0.00391	0.01214	0.01449	0.00312	0.00424
P41 - Blade2.FD1020	0.00119	0.00563	0.00077	0.00835	1.00000	0.02052	0.00170	0.00325	0.04260	0.02451	0.00501	0.01357	0.00665	0.03937	0.00598	0.00541	0.04512	0.00554	0.00724	0.00839
P42 - Blade2.FD1021	0.00518	0.00053	0.01171	0.07267	0.03925	1.00000	0.00195	0.00108	0.00112	0.00653	0.02006	0.01471	0.00146	0.02484	0.03057	0.00920	0.02699	0.20505	0.55919	0.56200
P43 - Blade2.FD1022	0.01846	0.02174	0.00051	0.00517	0.00081	0.05545	1.00000	0.01408	0.00470	0.00119	0.01019	0.01984	0.00077	0.00253	0.00365	0.00274	0.00277	0.02578	0.06357	0.06330
P44 - Blade2.FD1024	0.00013	0.00105	0.00077	0.00419	0.00030	0.03031	0.00551	1.00000	0.00682	0.00090	0.00320	0.00332	0.05720	0.01235	0.00492	0.08209	0.00358	0.09166	0.36114	0.36398
P45 - Blade2.FD1026	0.02218	0.00020	0.00014	0.00096	0.02702	0.04090	0.00258	0.00073	1.00000	0.00755	0.00200	0.00019	0.00747	0.06118	0.00064	0.01922	0.02499	0.40921	0.03691	0.03162
P46 - Blade2.FD1027	0.00159	0.00010	0.00021	0.00763	0.03652	0.00243	0.00228	0.00118	0.00127	1.00000	0.00051	0.00107	0.00351	0.00089	0.00014	0.04030	0.02247	0.01403	0.00074	0.00022
P47 - Blade2.FD1028	0.01018	0.00279	0.00048	0.02275	0.00664	0.01372	0.00373	0.04411	0.00418	0.03621	1.00000	0.00046	0.02607	0.14906	0.01774	0.00157	0.00254	0.09794	0.00146	0.00008
P48 - Blade2.FD1029	0.00415	0.00162	0.00064	0.00671	0.00087	0.00334	0.00116	0.00919	0.04545	0.00519	0.00289	1.00000	0.02491	0.03554	0.02120	0.00100	0.02922	0.00838	0.00671	0.00519
P49 - Blade2.FD1030	0.00393	0.06860	0.00267	0.00584	0.00822	0.01413	0.01122	0.01221	0.03031	0.01819	0.02416	0.01312	1.00000	0.01864	0.00361	0.00840	0.00647	0.02103	0.00076	0.00035
P50 - Blade2.FD1031	0.00043	0.00643	0.00116	0.00848	0.00404	0.00369	0.02176	0.00371	0.00910	0.01515	0.00143	0.06040	0.00203	1.00000	0.05326	0.00488	0.03485	0.01017	0.01845	0.01764
P51 - Blade2.FD1032	0.00137	0.01443	0.00633	0.04389	0.01139	0.02665	0.04031	0.01765	0.00071	0.00825	0.00293	0.01707	0.00354	0.00101	1.00000	0.00018	0.03243	0.00297	0.00714	0.00721
P52 - Blade2.FD1034	0.00289	0.00261	0.00029	0.02656	0.00011	0.07142	0.00041	0.00598	0.00459	0.00061	0.00333	0.01409	0.03067	0.00477	0.00064	1.00000	0.00839	0.03096	0.02986	0.03219
P53 - ExportPoints1.FD1	0.08496	0.01120	0.00516	0.00460	0.00761	0.01962	0.00013	0.00308	0.02247	0.00489	0.02484	0.00007	0.01166	0.00042	0.02508	0.01169	1.00000	0.04172	0.00989	0.01319
P18 - VTF etas tt	0.00292	0.00003	0.02596	0.00707	0.00943	0.15145	0.01765	0.09453	0.66946	0.01356	0.11284	0.00935	0.04629	0.00863	0.00772	0.00465	0.03514	1.00000	0.28958	0.34605
P19 - VTF power	0.00074	0.00052	0.01120	0.00253	0.00926	0.55314	0.05035	0.36443	0.01838	0.01711	0.00607	0.00294	0.02622	0.03459	0.00448	0.04374	0.01630	0.44172	1.00000	0.99421
P20 - VTF pr tt	0.00079	0.00052	0.01713	0.00221	0.00900	0.55591	0.04950	0.37556	0.00645	0.02235	0.00405	0.00299	0.03557	0.02901	0.00488	0.03995	0.01812	0.48956	0.99417	1.00000

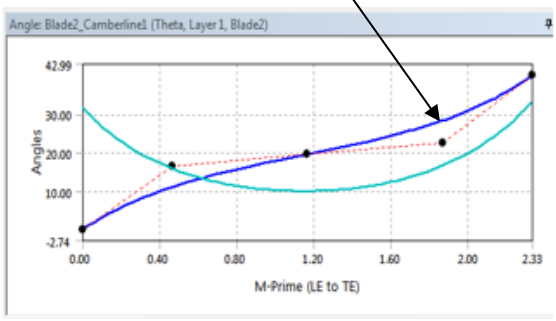

The connections between the input parameters, establish to what extent the conditions of the objective function are respected, thus for each optimization method applied, various candidates considered to be suitable for generating an optimal rotor geometry were obtained. The values of these parameters are mentioned in Table 6.6. Comparing the output data (power, pressure ratio, isentropic efficiency), leads to the choice of the *500_C1_Screening* candidate as the optimal candidate of this analysis. An important aspect in its selection is the value of the power consumed, being 2.05% lower than that of the candidate *100_C2_Screening* (for which the highest efficiency is calculated).

6.2. Comparative analysis of numerical simulations

Figure 6.4 describes the process used to determine an optimal configuration of the centrifugal impeller, process that is constrained by the input conditions and the impeller constraints. The preliminary dimensioning is based on 1D meanline design, representing the turbomachinery fundamental flow relationships supplemented by empirical correlations. This stage represents the basis of both sizing methods used, being later completed with additional methods, aiming to obtain a first approximation of the rotor's performance. In order to verify these results and compare to what extent the 1D model and the inviscid calculations provide a

true approximation of the performances, numerical modeling were performed for the geometries considered optimal by the objective function (*500_C2_MOGA* and *500_C1_Screening*). A final stage of the calculation methodology is the comparison of the data obtained from the numerical modeling with the data obtained in the geometric optimization stage.

Table 6.6 – Performance validation for candidates considered optimal

	P53 - ExportPoints1.FD1	P18 - VTF etas tt	P19 - VTF power (W)	P20 - VTF pr tt
max	15	0.88651	7.2376	1.7014
100_C2_Screening	9	0.8848	64528.9	1.6148
100_C3_MOGA	13	0.8837	63362.1	1.6009
500_C1_Screening	9	0.8836	63206.2	1.599
500_C2_MOGA	9	0.8838	63553.3	1.603
min	9	0.80689	4.0397	1.3252

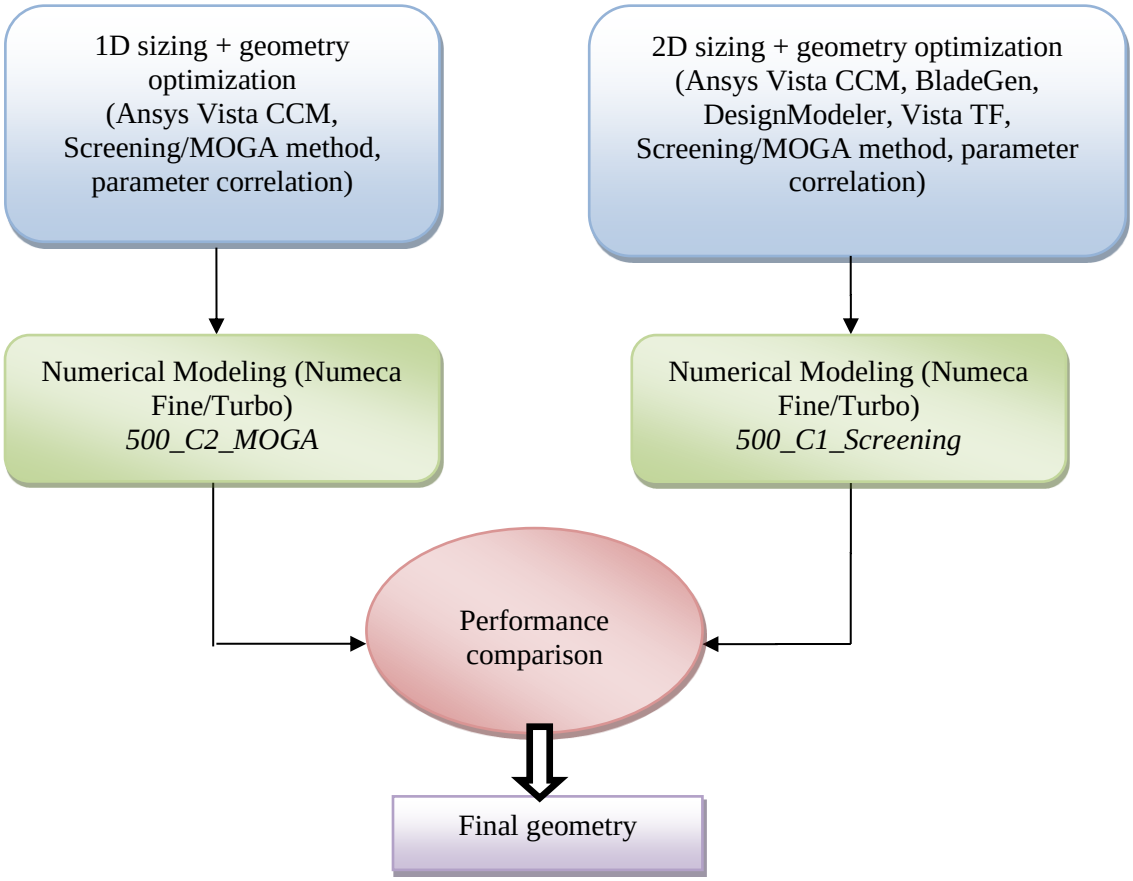

Fig. 6. 4 – Optimization process for an impeller configuration

Figure 6.5 highlights the geometrical differences between the two impellers, corresponding to the candidates resulting from the 1D and 2D sizing and optimization process. The major

differences are observed towards the trailing edge of the blade, but if we analyze the geometrical variation on the blade height, the geometric differences are also visible for the leading edge, Fig.5b).

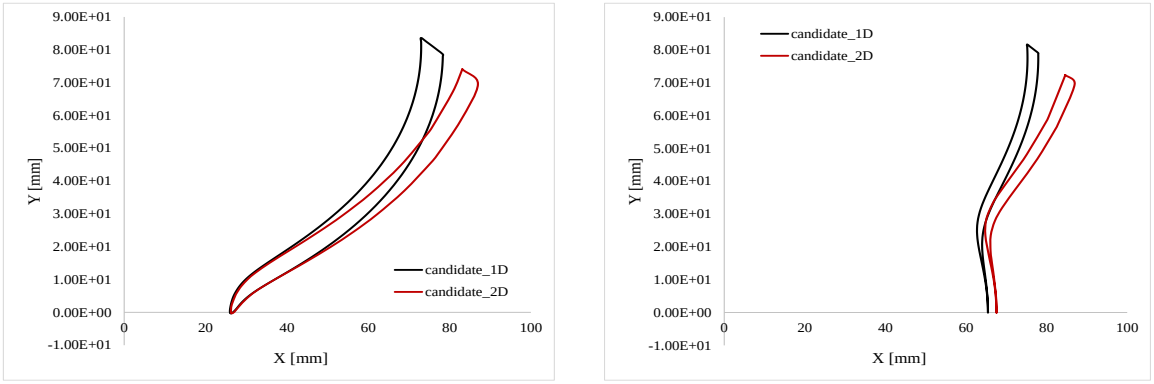

a) hub b) shroud

Fig. 6.5 – Geometrical differences between the two candidates result in the optimization process

The steps preceding the actual analysis are carried out respecting the characteristics identified in the study from Chapter IV. The computational grid was realized with the help of the Numeca/Fine Turbo program, consisting of a blocking scheme (hexahedral topological isomorphism). Being a structured grid, inflation near the blade was assured and also the value of $y+$ was maintained near one unit, in order to capture of the phenomena that appear in the turbulent boundary layer. For boundary conditions imposed correspond to the nominal point, the inlet was set at total pressure (101353 Pa) and total temperature (293 K), while for the outlet domain mass flow rate (3500 Nm3/h (1.19 kg/s)), having as a working fluid compressible ideal gas. All walls were considered adiabatic and without slip. Second order central difference schemes were used throughout the campaign. The numerical simulations were based on RANS steady - state study using the k – ω SST turbulence model.

The graph presented in Fig. 6.6 presents, in percentages, the differences between the two numerical analyses, exhibiting which are the parameters most influenced by the geometrical changes made. Thus, the exit flow angle is the parameter for which the major difference between the methods was obtained, and in addition to the rest of the changes made to the parameters, it leads to the geometric and performance differences between the two optimization methods. In terms of rotor performance evaluation, there is a 2.145% increase in efficiency in the case of the 2D sizing analysis and a 2.04% decrease in power for the same analysis. In evaluating the pressure ratio, the difference between the two models is small, below 0.015%. Based on these results, it can be stated that the 2D optimization process, which involves parameterizing the rotor blade, leads to higher rotor performance.

Apart from this step of comparing the results of the two CFD analyses, it is also necessary to compare them with the results obtained in the optimization process, to determine to what extent an optimization calculation can determine the performance of a rotor.

Figure 6.7 compares the results of the calculation stages with each other, as follows: 1D dimensioning analysis vs. 2D dimensional analysis and 3D numerical modeling for 1D geometry vs. 2D geometry. According to this graph, by comparing the two geometries for the numerical modeling process (3D), differences of up to 3% are obtained between the

performances of the two configurations. But when comparing the geometry dimensioning models, the differences double for some parameters, reaching 5% in the case of the pressure ratio. The 1D sizing model leads to higher performance values; this being a simple model based on fundamental turbomachinery theory together with specific empirical correlations without considering loss modeling. The 2D model, in turn, is based on conservative corrections (Euler model together with losses approximations in the boundary layer), thus the performance calculation is achieved with a higher accuracy.

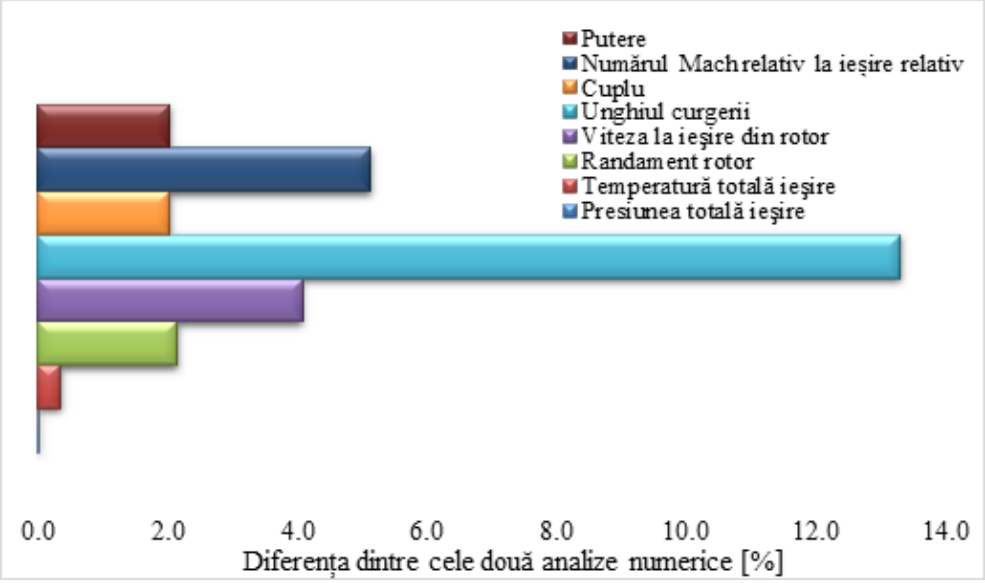

Fig. 6.6 – Differences between parameters of interest for the two candidates (*500_C2_MOGA* and *500_C1_Screening*)

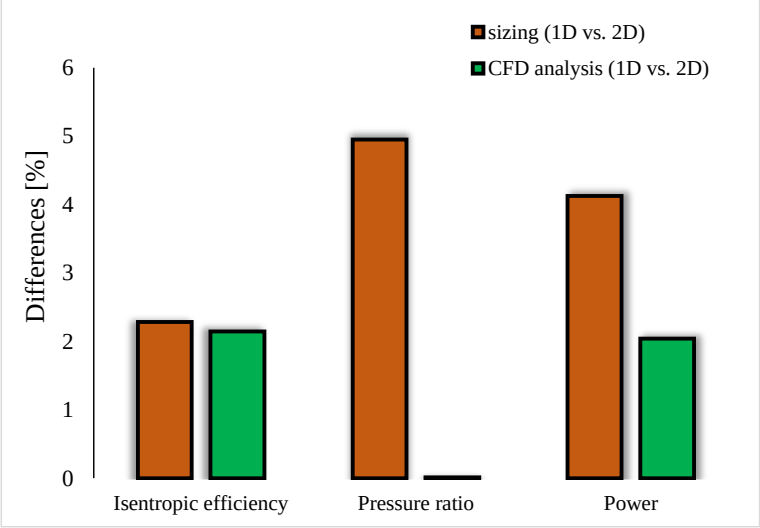

Fig. 6.7 – Comparison of the impeller sizing results (1D vs. 2D), numerical modeling (1D vs. 2D)

Figure 6.8 presents the differences between the three impellers: the shrouded impeller rotor (existing on the centrifugal blower), the 1D the unshrouded impeller developed through the 1D sizing process (optimization process - Screening methods, MOGA, parameter correlation) and the unshrouded impeller developed through the 2D sizing process (BladeGen, DesignModeler, inviscid analysis - Euler model, Screening and MOGA methods and parameter correlation).

The differences in the performance parameters are up to 8%, the impeller optimization leading to the increase of the consumed power, this value being obtained when comparing the power of the shrouded impeller with the unshrouded impeller obtained through 1D sizing. Optimizing the geometric configuration of the rotor contributes a fairly large percentage to the energy efficiency of the blower, by increasing efficiency by up to 7% (geometry corresponding to the 2D dimensioning model).

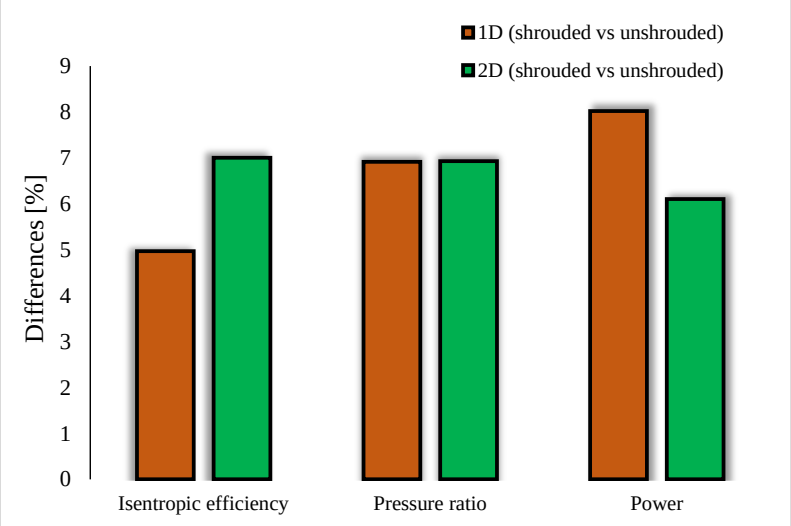

Fig. 6.8 – Performance comparison between the shrouded impeller and the two optimized unshrouded impellers

Preliminary conclusions

Chapter 6 presents the design and optimization process of a radial impeller, representing an integrated part of a 3500 Nm^3/h blower assembly. The baseline impeller was shrouded and developed with fundamental design equations, leading to a low efficiency (88%), compared to the new performances that can be obtained for radial impellers. Therefore, this chapter presents the process of dimensioning and optimization of an unshrouded impeller to satisfy design requirements corresponding to the centrifugal blower.

In order to obtain an optimal configuration of the impeller, two dimensioning and optimization methods were used:

a) method based on 1D sizing using ANSYS Vista CCM, followed by the optimization stages, which involved establishing the important parameters that influence the impeller geometry, imposing an objective function leading to obtaining the desired results from the rotor (pressure ratio, low power, high efficiency) and the correlation process of the parameters involved in defining the rotor geometry;

b) 1D dimensioning, followed by small changes to the geometry in BladeGen (leading edge and leading edge shape, blade angle, blade thickness, etc.), geometry parameterization in DesignModeler, penalty function settings, direct optimization process and parameter correlation.

Based on the optimization process, a series of candidates that satisfy the imposed objective function (highest efficiency, lowest power) were obtained, and among them one candidate was selected for each optimization method. The performances obtained for the two candidates are

subsequently compared with the results obtained from the 3D numerical analysis, corresponding to these candidates. In the comparison of the results obtained for the 1D dimensioning model and the 2D sizing model, the performance parameters were overestimated by the 1D (theoretical) model by up to 5% in the case of the pressure ratio. This overestimation is due to the lack of loss assessment models and a succinct description of the flow due to the model.

Discrepancies also exist between the results obtained from the 2D dimensioning model and the 3D numerical modeling of the geometry; up to 9% for the pressure ratio; making the pressure ratio the most overrated parameter in this analysis.

In the comparison of the 3D CFD results (corresponding to candidates *500_C2_MOGA* and *500_C1_Screening*) the differences are much smaller, up to 2.4% for the pressure ratio. The use of a full numerical model, RANS type coupled with the $k-\omega$ SST turbulence model led to a more accurate assessment of fluid flow in the rotor channels and performance evaluation.

The success of the optimization process depends on several elements, the most important being: the simplicity and clarity of the penalty function, the sampling of the space of free parameters, as well as the accuracy of the assessment of individuals. The objective function used can be adapted according to the requirements and the realities of the case studied (it must remain realistic), while the sampling and the accuracy of the assessment of individuals are dependent on the available resources. Therefore, a balance must be considered between modeling accuracy and the minimum number of samples required for the actual optimization.

CHAPTER VII

VALIDATION OF NUMERICAL MODELING THROUGH EXPERIMENTAL RESEARCH

The validation of the modeling presented in Chapter VI usually involves comparing numerical data with those obtained from an experimental campaign. But there is also the possibility of verifying them through the validation of the mathematical model, applied in the numerical simulation process. And for its validation, the experimental data of several existing geometric cases in the specialized literature are compared with the numerical ones, obtained after the numerical simulation. Such a study was also carried out in Chapter V, and the obtained results confirm that the numerical methods used are able to determine quite precisely the performances of an impeller, regardless of whether they are evaluated at the nominal point or off-design.

7.1. Model validation – case I

In addition to the previous statement, and for further confirmation of the results of the numerical modeling process, are presented the results of the centrifugal blower with the shrouded impeller, both experimental data and numerical analysis.

The 3500 Nm^3/h turbo blower that represents the basis of this research, is part of the props of NRDI COMOTI, being developed in a project that aimed to design and test a centrifugal blower used in industrial wastewater treatment plants. The 3500 Nm^3/h blower assembly is exhibit in Fig. 7.1 and highlights the blower on the experiment test rig (a, b), and a part of the probes used for instrumentation (a, b).

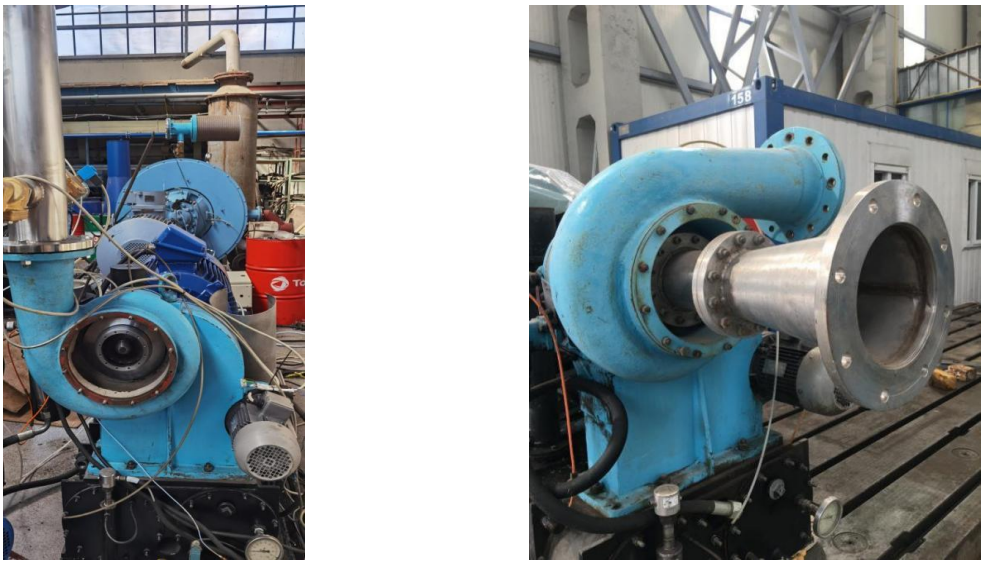

a) b)

Fig. 7.1 – The 3500 Nm3/h blower assembly on the experimental test rig

Figure 7.2 indicates the differences between the experimental data *(***Comoti, 2008)* and the numerical results obtained from the CFD analysis. According to these data, the differences between the two cases are below 3%, which represents a validation of the applied CFD model. The major difference between the results is obtained for the lowest pressure, namely 1.5 bar. As the pressure increases this difference decreases, with a value below 1% for a pressure of 1.6 bar. The numerical simulations realized for these cases are more accurate for the working points close to the design point of the blower. Therefore, the differences obtained around the nominal point are the smallest; the numerical simulations properly estimating the performance of the blower.

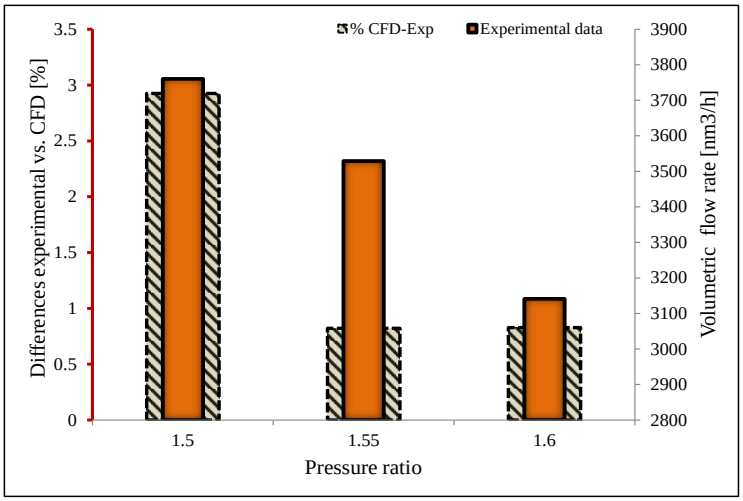

Fig. 7.2 – CFD – experimental comparison of pressure ratio

7.2. Model validation – case II

In support of the numerical analyzes presented in Chapter VI, an additional analysis of a compressor used for underground gas storage was carried out. By means of the analysis described in the following, it is desired to emphasize the accuracy of the CFD process, being presented an analysis carried out by similarity, for high energy efficiency equipment.

The theme of the project was to develop a compression stage with the highest possible efficiency, which would meet the following requirements: outer diameter 350 mm, suction pressure between 10 and 12 bara, maximum rotational speed 24000 rpm and a minimum pressure ratio of 1.55 *(***Comoti, 2006)*, and methane as the working fluid.

The experimental tests for this compressor were carried out under similarity conditions, using air as the working fluid, according to PTC10 norms - ASME, respectively ISO 5389 *(***Comoti, 2006)*. Figure 7.3(a) presents the assembly of the centrifugal rotor, together with a detail regarding the pressure samples used in the instrumentation of the vaned diffuser Fig. 7.3(b).

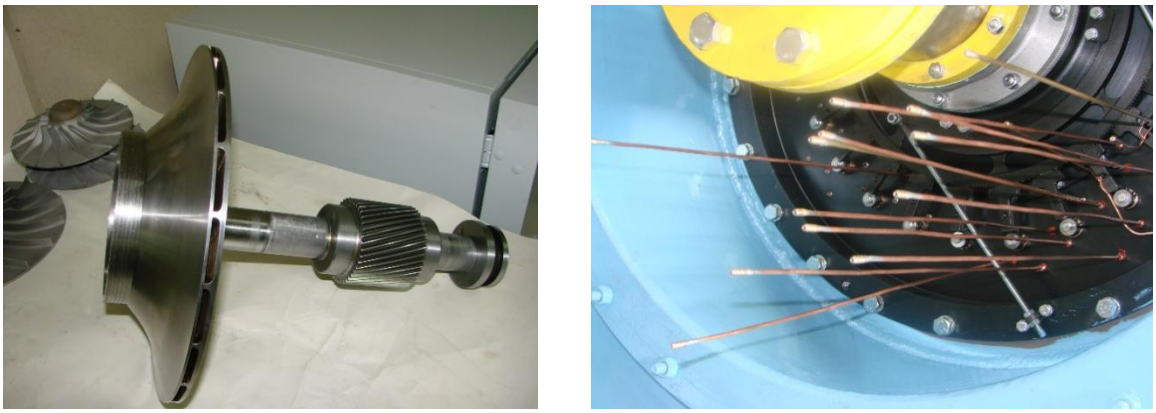

a) b)

Fig. 7.3 – Centrifugal compressor equipment *(Gherman, Dumitrescu, &Nitulescu, 2018)*

The similarity point for which the experimental tests were carried out corresponds to the speed of 14915 rpm, total inlet pressure 0.9995 bar, total temperature 27°C and a flow rate of 0.437 kg/s. The evolution of the fluid in the compression stage is presented by means of parameters considered important for the operation of the compressor.

The total pressure distribution in the compression stage is illustrated in Fig. 7.4. Its variation is uniform around the circumference, showing an increase as the fluid moves towards the impeller exit. Once the fluid reaches the vaned diffuser, there is a slight decrease in total pressure, reaching a value of 1.73 bar in the discharge area.

Mach number representation at 50% of blade height, Fig. 7.5, shows a subsonic flow in the impeller, without boundary layer separations. The average value of the impeller outlet Mach number is 0.594 and decreases to 0.19 at the diffuser discharge.

The comparison of numerical results with experimental data was carried out based on the pressure values. Regarding the fluid flow pattern in the impeller, the CFD analysis correctly estimates the pressure losses, with a difference of less than 2.5%. As for the vaned diffuser, the pressure values obtained in the inlet and discharge area of the domain were compared, the

results being represented in Fig. 7.6. At the diffuser inlet, the discrepancies are up to 5%, but reaches 7.6% for the diffuser discharge. The CFD model overestimates the total pressure, and this may be due to the turbulence model used and the RANS model, which cannot estimate the losses in the diffuser with great accuracy. But for a RANS model, with a limited number of grid cells, the differences are considered to be acceptable.

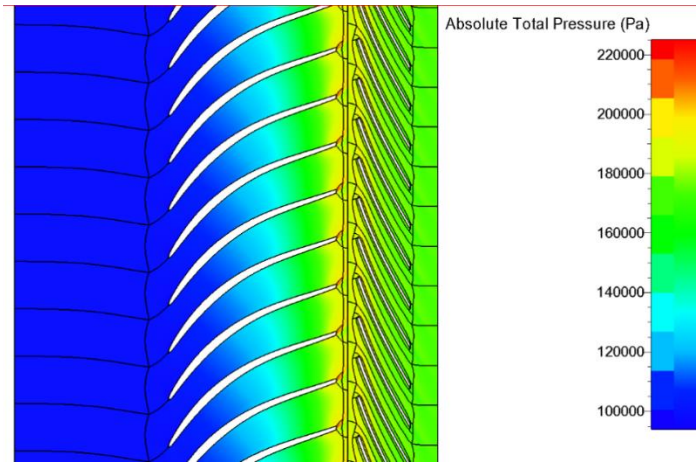

Fig. 7.4 – The total pressure in the compression stage

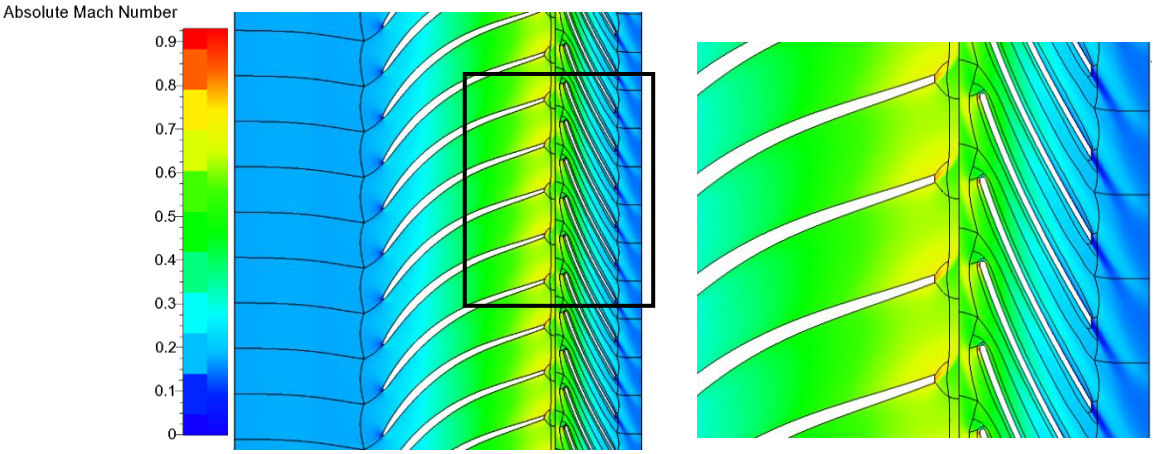

Fig. 7.5 – Mach number in the compression stage

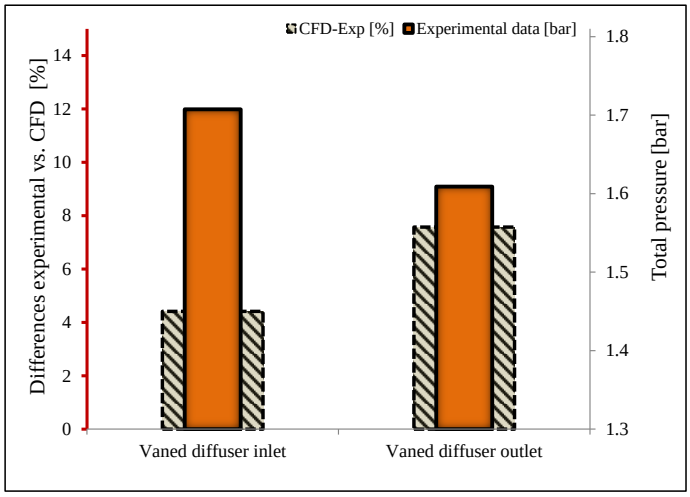

Fig. 7.6 – Comparison of CFD – Experimental for the vaned diffuser

7.3. Energetic efficiency

The present paper joins the studies from the specialized literature in the field of centrifugal turbomachines, through its attempt to participate in their energy efficiency. The high energy consumption associated with air blowers and compressors, along with increasing energy prices, make these equipment ideal candidates for research, with a view to improve and reduce life cycle costs.

Energy and maintenance costs represent the largest part of the costs associated with the life cycle of an air compression equipment. Among the factors that contribute unfavorably to the increase in energy costs are: using the system at an incorrect pressure, which contributes both to the increase in energy consumption and to financial losses; air losses in the system that negatively influence power; operation of the compressor at idle without compressing air; low air quality at the equipment entrance; incorrect or incomplete design of the system that can lead to the reduction of its efficiency, etc. In addition to the factors mentioned, there are others that contribute particularly to high maintenance costs.

The study carried out in this paper aimed to replace the existing rotor with an optimized version of it, which would ensure an increase in the efficiency of the blower, for a power consumption as low as possible. The numerical optimization process based on the optimization of the blade shape, led to an increase in the impeller efficiency by up to 7%, but this increase in efficiency is followed by a rising in the power consumed by the blower. However, the new rotor configuration ensures for the same operating conditions, an increase in the pressure ratio by 6.93%, improving the operating range of the blower. Thus, the sizing and optimization methodology described in this paper contributes to the energy efficiency of centrifugal compression equipment.

Such an optimization process, carried out taking into account the specific constraints of the blower/compressor operating range, can ensure the decrease of pressure losses in the equipment, the increase of the efficiency and/or the increase of the operating range, but also the increase of the life of the equipment, which leads to lower financial costs. It is also important to establish from the design stage if the purpose of the compression equipment is:

- long operation at maximum efficiency, meaning lower consumed power and implicitly reduction of CO_2 emissions;
- wider operating range, but with lower performances;
- both of them, which will require the use of an optimization procedure, such as the one described in this paper, to ensure the sizing of such equipment.

CHAPTER VIII

GENERAL CONCLUSIONS, ORIGINAL CONTRIBUTIONS AND FUTURE PERSPECTIVES

The doctoral thesis entitled ***Energy efficiency of turbomachine design and operation*** aimed to determine a way to increase the efficiency in the field of centrifugal blowers by means of CFD simulations correlated with numerical optimization methods based on genetic

algorithms. Establishing such a method is an important step in the field of turbomachines, which represent some of the world's largest energy consumers, but also an attractive target for improving energy efficiency.

The doctoral thesis was structured in eight chapters in order to fulfill the general objectives and the specific objectives defined in Chapter I, namely the development of a methodology for sizing radial impellers by means of genetic algorithms, establishing the importance of optimization methods and the parameters involved in the process, defining the importance of numerical modeling stages and validating the mathematical model applied in the numerical modeling process, with the help of experimental data.

The general conclusions resulting from the research study are the following:

- Numerical modeling represents an essential method for determining the performance of turbomachines, constituting a much faster way of obtaining a configuration, benefiting at the same time from low costs and the lack of recurring experimental campaigns.

In Chapter IV, the importance of the numerical simulation stages was established, the study being focused on determining the mesh influence on the centrifugal impeller pressure ratio and efficiency. In addition to the four different grid resolutions: 0.7 million, 1.5 million, 5 million and 9 million, the impact of turbulence models on performance was also analyzed. Four turbulence models are used for this aspect: Spalart – Allmaras, *v2f*, k-ω Shear Stress Transport (RANS and URANS) and Explicit Algebraic Reynolds Stress Model (EARSM). As a result of the study, it was found that for a grid size greater than 1.5 million elements per channel, numerical instabilities appear and the convergence time is longer. The Spalart - Allmaras model provides a higher-pressure ratio, but a slightly lower efficiency compared to *SST*; while the *EARSM* model offers a higher efficiency and pressure ratio than all other models tested. This has been interpreted as a problem with the explicit algebraic formulation of *EARSM* that negates the advantages of the method.

All these characteristics of numerical modeling are limited by the calculation costs and the level of accuracy of the obtained solution; thus establishing a method leading to a maximum level of precision allowed by RANS modeling, with a reduced computational effort, was the priority of this research.

- Validation of the numerical calculation model, by comparing some experimental data, representative from the specialized literature, with the CFD results corresponding to the respective configurations, led to obtaining a maximum difference of 9%, in determining the performances. This difference being obtained for off – design conditions. For the impeller that assures low pressure ratios, closed to 1.1 – 1.2, the CFD analysis provides results of higher accuracy, below 1% in assessing the pressure ratio and below 3% for the isentropic efficiency.

Thus, it was considered that although changes can be made to this model, there will always be an error between experimental and CFD. Both mathematical models, are limited by a number of factors, such as: boundary and initial conditions, turbulence modeling, heat transfer, etc., as well as the impossibility of manufacturing the exact geometrical model calculated (depends on the geometric complexity and the manufacturing method) that may lead to differences between different performance evaluation methods.

- Defining a method for dimensioning the geometry of a radial impeller based on the correlation of 1D and 2D preliminary design, empirical correlations and genetic algorithms.

The 1D sizing only establishes the geometric parameters of the impeller and the shape of the working channel, while the 2D process allows also changes to the blade profile. Correlating these stages together with the optimization procedure can lead to minimizing losses, increased efficiency or wider operating range.

Another important objective of this research is the establishment of some correlations between the parameters involved in the optimization process, through which their influence on the impeller geometry is determined, but also the way in which those parameters influence each other.

At the same time, the importance of the number of samples used in determining the optimal geometry was also analyzed. According to this study, the number of samples provides a more thorough analysis of the domain, taking into account more geometric possibilities.

The optimization methods, Screening or MOGA, present two different ways of determining the values of the geometric parameters, so as to lead to the most optimal geometry based on the constraints imposed. Of the two methods, MOGA is based on multi-objective searches, performing simultaneous optimization of several objectives, while the Screening method searches the intended domain and chooses the most suitable solutions.

- Validation of the numerical simulations realized for the shrouded impeller, by comparison with experimental data, support the results obtained in its dimensioning. The comparison between the two evaluation methods, carried out at the nominal point, offers a difference of less than 1%, but this value increases for off design conditions.

To support the evaluation of the CFD model, an additional comparison with experimental data corresponding to a centrifugal compressor designed to operate with methane was carried out. The comparison was made under similarity conditions, and the discrepancies between the two methods are up to 2.5% for the rotor and below 8% for the measurements made in the vaned diffuser.

From a scientific point of view, the contributions of this research establish a methodology for sizing and optimizing radial impellers using genetic algorithms. Also, the numerical validation carried out by comparing with experimental data, together with the study on the grid influence, the numerical scheme and the turbulence model can constitute a solid basis in choosing the characteristics corresponding to a RANS analysis that reflects the experimental values as accurately as possible.

The use of CFD-based numerical analysis has had a great economic impact since its inception. The increase in computing power led to obtaining the geometric configurations corresponding to the turbomachines, in a shorter time, avoiding additional costs necessary for iterative experimental testing of the products. Therefore, the use of optimization methods has a significant impact on large industries, especially on manufacturers, offering reduced costs and shorter time to obtain the final product.

In recent years, the impact on the environment is one of the primary aspects taken into account in the development of a new product or the rehabilitation of existing ones. In order to meet the increasingly strict requirements in this field and implicitly reducing gas emissions, methods are used to optimize the components of the blowers, such as the one described in this

paper, obtaining either the highest operating efficiencies or the widest possible working range, but with power requirements as low as possible.

8.1. Personal contributions

The doctoral thesis contains a vast study on the energy efficiency of centrifugal turbomachines, more precisely in the field of blowers/compressors, encompassing both known notions and original contributions, adding novelty to the topic addressed. The personal contributions that can be found in this thesis are the following:

- Synthesizing information regarding the current state of research in the field of centrifugal radial machines, both from a constructive point of view and the calculation methods used in their development;
- Carried out a study on the influence of the mesh resolution, the numerical scheme and turbulence models, in evaluating the performances of a centrifugal compressor, as well as establishing the links between them;
- Defining the numerical analysis methodology, applying it to the studied cases and interpreting the results, in order to establish the accuracy of the solution;
- Development of a methodology to evaluate and validate the performance of a radial rotor, based on the comparison of experimental data with numerical CFD results, corresponding to several different types of rotors. The compressor characteristic map was also plotted for these configurations, with both experimental and CFD data highlighting how the numerical model influences the pressure ratio and isentropic efficiency of the working machine.
- Defining a methodology to optimize the dimensioning process of centrifugal impellers, by comparing two sizing methods (the first method based only on the optimization of the global parameters that define the rotor and the working channel, the second method based on the optimization of the blade shape). Carrying out a comparison between the MOGA and Screening optimization methods; also, for the two methods was realized a comparative analysis studying the influence of the number of samples used in searching in for the optimal parameters.
- Perform modeling and numerical simulations for two types of radial impellers (shrouded and unshrouded) and demonstrate why the impeller without front shroud are more efficient.

8.2. Future research directions

The studies carried out in this paper are associated with the achievements in the field of centrifugal turbomachinery research, but this is a complex field with a high level of interdisciplinary, its continuous development being always possible, thus identifying the following directions for further development of the works:

- Carrying out an LES-type numerical analysis for the geometry obtained in this research and comparing the results obtained with the RANS model, in order to determine how large the difference between the two models is, in terms of accuracy of the results, for such a case. Completing the analysis with a study of the computational effort (hardware and time frame) relative to the level of accuracy of the results.

- Dimensioning a customer - made volute for the obtained impeller.
- Experimental testing of the centrifugal blower and validating further the numerical data. Thus, realizing a methodology for designing a blower/centrifugal compressor that allows obtaining a final configuration, optimal for the field of use in the shortest possible time.

PUBLISHED PAPERS

I. Published papers in ISI ranked journals

1. Valeriu Drăgan, **Oana Dumitrescu**, Ion Mălăel, Adrian Daniel Azoiței, Rake impact on turboshaft compressors, a numerical study, Aircraft Engineering and Aerospace Technology, ISSN: 0002-2667, 2020, (impact factor 1.478)

II. Published papers in ISI indexed journals

1. **Oana Dumitrescu**, ValeriuDrăgan, IonutPorumbel, Bogdan Gherman, Numerical assessment of a very high pressure ratio centrifugal impeller, IOP Conference Series Materials Science and Engineering 916(1):012035, 2020
2. **Oana Dumitrescu**, ValeriuDrăgan, Bogdan Gherman, Aerodynamic development of a high-pressure ratio compressor for an advanced microturbine powerplant, IOP Conference Series Materials Science and Engineering 916(1):012034, 2020
3. Adrian Stoicescu, **Oana Dumitrescu**, Gheorghe Fetea, Automated Multi-Reference Control for Centrifugal Compressor, *2019* International Conference on ENERGY and ENVIRONMENT (CIEM), 2019, pp. 167-171, doi: 10.1109/CIEM46456.2019.8937654
4. **Oana Dumitrescu**, Bogdan Gherman, AndreeaAlcea, Tip clearance influence in CFD calculations and optimization of a centrifugal compressor stage through CFD methods, IOP Conference Series: Materials Science and Engineering, Volume 400, Issue 4, 2018
5. Bogdan Gherman, **Oana Dumitrescu**, Marian Nitulescu, Numerical and experimental evaluation of a centrifugal compressor, IOP Conference Series: Materials Science and Engineering, Volume 400, Issue 4, 2018
6. ValeriuDrăgan, **Oana Dumitrescu**, Ion Mălael, IonuţPorumbel, Bogdan Gherman, Cristian Puşcaşu, Turbulence model sensitivity on steady state mapping of a very high pressure ratio compressor stage, AIP Conference Proceedings 2046, 020024, 2018

III. Published papers in ISI indexed journals in fields related to the doctoral thesis

1. Mihaela Raluca Condruz, **Oana Dumitrescu**, Tiberiu Frigioescu, Razvan Cârlănescu, C Dumitru, A. Ghinea, Solidification simulation and casting of an impeller designed for a thermochemical treatment furnace, AIP Conference Proceedings 2302, 120001, 2020; https://doi.org/10.1063/5.00336622
2. Bogdan Gherman, **Oana Dumitrescu**, Valeriu Dragan, Transonic flow study in a centrifugal compressor using perforated airfoils, Bulgarian Academy of Sciences. Space Research and Technology Institute. Aerospace Research in Bulgaria. 32, 2020, DOI: https://doi.org/10.3897/arb.v32.e10

IV. Published papers in international database indexed journals

1. **Oana Dumitrescu**, Ionuț – Florian Popa, design and optimization of a centrifugal pump as part of mechanically pumped fluid loop cooling system for spacecraft, U.P.B. Sci. Bull., Series D, Vol. 83, Iss. 3, 2021, ISSN 1454-2358

SELECTIVE BIBLIOGRAPHY

Ali, Z., Tucker, P., & Shahpar, S. (2016). Optimal Mesh Topology Generation CFD. Computer Methods in Applied Mechanics and Engineering 317.

Belhi, M., Deligant, M., Podevin, P., & Khelladi, S. (2013). Inverse methodology for centrifugal compressor design using genetic algorithm. BulTrans-2013 Proceedings.

Chen, X., & Agarwal, R. (2013). Shape Optimization of Airfoils in Transonic Flow Using a Multi-Objective Genetic Algorithm. Journal of Aerospace Engineering, 228, (pg. 1654-1667).

Drăgan, V., Dumitrescu , O., Mălăel, I., Porumbel, I., Gherman, B., & Puşcaşu, C. (2018). Turbulence model sensitivity on steady state mapping of a very high pressure ratio compressor stage. ICNPAA 2018: Mathematical Problems in Engineering, Aerospace and Sciences, American University of Armenia (AUA). Yerevan.

Galerkin, Y., Voinov, I., & Drozdov, A. (2017). Comparasion of CFD calculations of centrifugal compressor stages by NUMECA Fine Turbo and ANSYS CFX programs. IOP Conf.Series Materials Science and Engineering 232.

Gherman, B., Dumitrescu, O., & Nitulescu, M. (2018). Numerical and experimental evaluation of a centrifugal compressor. IOP Conf. Series: Materials Science and Engineering.

Gu, Y., Pei, J., Yuan, S., Zhang, J., & Wang, W. (2016). Multi-objective optimization of centrifugal pump impeller based on kriging model and multi-island genetic algorithm. 16th International Symposium on Transport Phenomena and Dynamics of Rotating Machinery.

Hasanbeigi, A. (2010). Energy-Efficiency Improvement Opportunities for the Textile Industry. Ernest Orlando Lawrence Berkeley National Laboratory.

Hataway, M. (1993). Experimental and Computational Investigation of the NASA Low-Speed Centrifugal Compressor Flow Field. NASA Technical Memorandum 4481.

Hirsch, C. (2007). Numerical Computation of Internal and External Flows: The Fundamentals of Computational Fluid Dynamics, second edition. Elsevier.

Ibaraki, S., Tomita, I., & Sugimoto, K. (2015). Aerodynamic Design Optimization of Centrifugal Compressor Impeller Based on Genetic Algorithm and Artificial Neural Network. Mitsubishi Heavy Industries Technical Review Vol. 52 No. 1.

Japikse, D. (1996). Centrifugal Compressor Design and Performance. Concepts ETI, Inc., ISBN 0-933283-03-2.

Norris, S. (2000). Chapter 2 - Finite Volume Differencing Schemes.

Oh, H., Yoon, E., & Chung, M. (1997). An optimum set of loss models for performance prediction of centrifugal compressors. Proceedings of the Institution of Mechanical Engineering Part A Journal of Power and Energy.

Parneix, S., Durbin, P., & Behnia, M. (1998). Computation of 3-D Turbulent Boundary Layers Using the V2F Model. Flow, Turbulence and Combustion, vol. 60, (pg. 19–46).

Rajakumar, D., Ramamurthy, S., & Govardhan, M. (2014). Experimental investigations on effects of tip clearance in mixed-flow compressor performance. Proceedings of the Institution of Mechanical Engineers, Part G: Journal of Aerospace Engineering.

Robinson, C., Casey, M., & Woods, I. (2011). An integrated approach to the aeromechanical optimisation of turbo compressors. ČKD Nové Energo & TechSoft Engineering.

Shaab, S. (2015). Design optimization of a centrifugal compressor vaneless diffuser. ELSEVIER, International Journal of Refrigeration, vol. 60, (pg. 142-154).

Syka, T., Matas, R., & Luňáček, O. (2016). Numerical and experimental modelling of the radial compressor stage. AIP Conference Proceedings 1745.

Stoicescu, A., Dumitrescu, O., & Fetea, G. (2019). Automated Multi-Reference Control for Centrifugal Compressor. International Conference on ENERGY and ENVIRONMENT (CIEM), pp. 167-171, doi: 10.1109/CIEM46456.2019.8937654.

Soo-Yong, C., Kook-Young, A., Young-Duk, L., & Kim, Y.-C. (2012). Optimal Design of a Centrifugal Compressor Impeller Using Evolutionary Algorithms. Hindawi Publishing Corporation Mathematical Problems in Engineering Volume 2012.

Timchenko, V., Tkachenko, S., Reizes, J., & Lau, G. (2016). Is comparison with experimental data a reasonable method of validating computational models? Journal of Physics Conference Series 745(3):032022.

Tosto, F. (2018). Investigation of performance and surge behaviour of centrifugal compressors through CFD simulations, Master's Thesis in Fluid Dynamics. KUNGLIGA TEKNISKA HOGSKOLAN, KTH Mechanics.

Wickerath, B., & Niehuis, R. (2006). A study of nonlinear eddy-viscosity models in a flow solver for turbomachinery. 25th International Congress of the Aeronautical Sciences.

Ziegler, K. (2003). Experimentelle Untersuchung der Laufrad-Diffusor-Interaktion in einem Radialverdichter variabler Geometrie. Dissertation RWTH Aachen.

ANRE. (2015). Model pentru întocmirea Programului de îmbunătățire a Eficienței Energetice pentru unitățile industriale în conformitate cu art.9 alin (3) lit. A) din Legea eficienței energetice nr. 121/2014. https://www.anre.ro/ro/eficientei-energetica/legislatie/. Accesat: Mai 2022

***Bakker, A. (2002). Lecture 5 - SolutionMethods, AppliedComputational Fluid Dynamics. Preluat de pe http://www.bakker.org

***Comoti. (2006). Raportul stiintific si tehnic. Programul Cercetare de Excelenta 2005 – 2008, Contract 753/2006.

***Comoti. (2007). Echipament de înaltă eficienţăenergetică,utilizat pentru înmagazinarea subterană a gazelor, în zonele care se confruntă cu dificultăţi în alimentarea cu gaze.Etapa II/Activitatea II.2. Elaborare Program de experimentare.

***European, C. (2022). Preluat de pe https://ec.europa.eu/clima/eu-action/climate-strategies-targets/progress-made-cutting-emissions_en

***Program, W. S. (2014). Premium Efficiency Motor SelectionandApplicationGuide, A Handbook for Industry. U.S. Department of Energy, Energy EfficiencyandRenewable Energy.